Korean Journal of Chemical Engineering
https://doi.org/10.1007/s11814-024-00235-w

REVIEW ARTICLE (INVITED ONLY)

Ligand Engineering for Indium-Based III–V Semiconductor Nanocrystals: A Review on Recent Process

Hyunwoo Jo[1] · Moon Sung Kang[1,2]

Received: 24 April 2024 / Revised: 12 July 2024 / Accepted: 19 July 2024

Abstract
This review provides a comprehensive overview of recent ligand engineering strategies for indium-based III–V semiconductor nanocrystals (NCs), focusing specifically on indium phosphide (InP) and indium arsenide (InAs). These materials have gained significant research interest as active substances compliant with the restriction of hazardous substances directive (RoHS) for advanced optoelectronic applications. Ligands attached to the NC surfaces play critical roles in determining the physical characteristics of the materials, including their structure, size, colloidal stability, electronic properties, and associated optophysical processes. Hence, practical applications of InP and InAs NCs require a good understanding of these ligands. Moreover, recent advances have demonstrated the importance of selecting appropriate ligands for enhancing the electronic and optical performances of InP and InAs NC-based electronic devices such as thin-film transistors, photovoltaic devices, photodetectors, and light-emitting devices. This review highlights the recent progress, technical challenges, and future directions in the context of ligand engineering to realize high-performance InP and InAs NC-based electronic devices.

Keywords Indium pnictogenides · Colloidal semiconductor nanocrystals · Ligand engineering · Electronic devices

Introduction

Colloidal semiconductor nanocrystals (NCs) synthesized in solutions by chemical methods have attracted attention because of their intriguing electronic and optoelectronic properties [1]. The quantum confinement effect of the NCs, effective when their size is smaller than the Bohr radius, enables precise control over the energy levels and associated excitonic transitions through simple tuning of NC size. The development of synthetic protocols has led to the production of NCs with high optical purities and luminescence quantum yields. In addition, NCs that exhibit optical absorption over a wide spectral range from ultraviolet (UV) to infrared (IR) have also been produced [2]. Accordingly, NCs are promising materials for (opto-)electronic devices such as light-emitting diodes (LEDs), photodetectors, photovoltaics (PV), and transistors [3]. While the benchmark NC systems developed from the early stage of research used toxic elements, such as Cd, Pb, or Hg, heavy metal-free NC systems that meet the restrictions of the hazardous substances directive (RoHS) regulations are being actively developed. Among these, indium pnictogenides, such as indium phosphide (InP) and indium arsenide (InAs) NCs, have been widely studied. InP NCs exhibit tunable emissive colors ranging from blue to deep red, leading to the successful integration of the materials in commercial "quantum dot" displays [4]. InAs NCs, which exhibit optical band gaps in IR regions and good transport characteristics, are attracting attention as key materials for IR-active electronic devices [5, 6].

Groups III–V semiconductors exhibit stronger covalent bonding characteristics than Groups II–VI or IV–VI semiconductors [7]. Hence, InP and InAs NCs, in principle, should exhibit higher structural stability than NCs with stronger ionic characteristics. However, their stronger covalent bonding characteristics imply that the synthesis of these materials would require higher temperature reaction conditions to decompose the precursors during colloidal synthesis, leading to challenges in obtaining well-controlled NCs. In addition, the energy level of the trap states originating from the dangling bonds at the surface atoms of these NCs

✉ Moon Sung Kang
kangms@sogang.ac.kr

[1] Department of Chemical and Biomolecular Engineering, Sogang University, 35 Baekbeom-ro, Mapo-gu, Seoul 04107, Korea

[2] Institute of Emergent Materials, Sogang University, 35 Baekbeom-ro, Mapo-gu, Seoul 04107, Korea

Published online: 27 July 2024

reside much deeper than those based on Groups II–VI or IV–VI semiconductors with stronger ionic characteristics [8]. Consequently, additional efforts are needed to passivate the structural defects that rarely appear in ionically bonded NCs and to boost the photoluminescence efficiency of Groups III–V NCs. Furthermore, because Groups III and V elements are highly oxophilic, they undergo severe oxidization when exposed to oxygen. This oxidized NC surface complicates atomistic surface investigation, requiring a separate process to remove the oxidized surface. Because of these issues, ongoing efforts focus on obtaining high-quality Groups III–V NCs for state-of-the-art electronic and optoelectronic device applications. The core of these efforts relies on a good understanding of the surfaces of NCs and the engineering of these surfaces.

The surfaces of colloidal NCs are typically capped with organic molecules, referred to as ligands. Ligands typically include a long hydrocarbon chain (tail group) attached to a functional group (head group) [9]. The head group binds directly to the NC surface atoms and passivates dangling bonds that produce trap states. According to the hard-soft acid–base theory [10], the head group bonds differently with the various surfaces of different NC systems. This highlights the importance of selecting an appropriate head group to ensure stable passivation and improved optoelectronic characteristics. The tail group of the ligands (directly included in the as-synthesized NCs) is generally composed of a long aliphatic chain, which helps stabilize the colloidal dispersion of the NCs in nonpolar solvents. The chemical nature of the tail group determines the type of solvents (non-polar solvents or polar solvents) in which NCs are dissolved and the solubility of NCs in solvents. Therefore, the processability of the NC depends on the chemical properties of the tail group. However, the long hydrocarbon chains are typically insulating. Hence, the electrical transport and charge/energy transfer characteristics are impeded by the tail group of the ligands. Therefore, ligands with long alkyl tail groups are often exchanged with short tails, either in the solution or solid phase, to effectively utilize NCs in optoelectronic devices. Overall, the engineering of NC ligands plays a crucial role not only in the synthesis of well-controlled NCs, but also in realizing optoelectronic devices with good processability and performance.

Herein, we review the recent progress in ligand engineering of InP and InAs NCs for utilization in NC-based electronic and optoelectronic devices. This review begins with a brief explanation of the various roles of ligands in NCs in terms of their synthesis, colloidal stability, surface passivation, and energy levels. In the following section, various strategies are introduced that are applied to the ligands of InP and InAs NCs to improve the performance of various NC devices including thin-film transistors (TFTs), photoconductors, PVs, and LEDs. Finally, future perspectives on the required ligand engineering to further advance the applications of InP and InAs NCs are discussed.

Roles of Ligands on Semiconductor NCs

Although the crystalline inorganic cores of NCs primarily determine their semiconductor properties, NCs cannot simply be classified as inorganic materials because they include a layer of organic ligands on the surface. This layer of ligands (assuming that the length of the molecules is 1 nm) accounts for up to 70 vol% of the material (assuming that the diameter of the inorganic core is 4 nm). In addition to volume uptake, they directly influence various aspects of NC characteristics. This section covers the various roles of the ligands on NCs during the synthesis of the material in enabling the colloidal stability of NCs in various solvents and modulating the electronic properties of NCs.

Influence of Ligand on the Synthesis of Semiconductor NCs

The synthesis of colloidal NCs is typically divided into two steps: nucleation and growth [11]. Nuclei are generated from supersaturated precursors during the nucleation step, and these nuclei grow further through the diffusion and adsorption of the precursors. The ligands included in the synthetic solution play critical roles, particularly in the later steps, and affect the size and shape of the resulting NCs (Fig. 1a). In particular, the tail groups of the ligands induce steric hindrance and affect the adsorption rate of the precursors, thereby changing the growth rate [12, 13]. Consequently, smaller NCs are typically formed as the length of the tail group increases. The contribution of the changes in the solubility and diffusivity of the precursors owing to changes in the tail group length should also be considered [14]. For example, longer ligands produce smaller NCs with an improved size distribution, particularly when carboxylic acid ligands of different lengths ($C_{10}H_{20}O_2$, $C_{14}H_{28}O_2$, and $C_{22}H_{44}O_2$) were employed for the synthesis of CdSe NCs. The result was attributed to the reduced solubility and diffusion coefficient of the precursors with increased carboxylic acid chain length [15]. When a similar experiment using ligands with an amine head group, which has weaker binding coordination than carboxylic acid, was carried out, the solubility and diffusion of the precursors were not strongly affected by the type of ligand used. Consequently, the size of the NC remained constant regardless of the changes in the length of the ligands.

The head group also plays an important role in determining the shape and morphology of NCs. For example, in the synthesis of PbS NCs, dodecanethiol (DDT) ligands prefer to adsorb on the (111) facet rather than on the (100) facet [16].

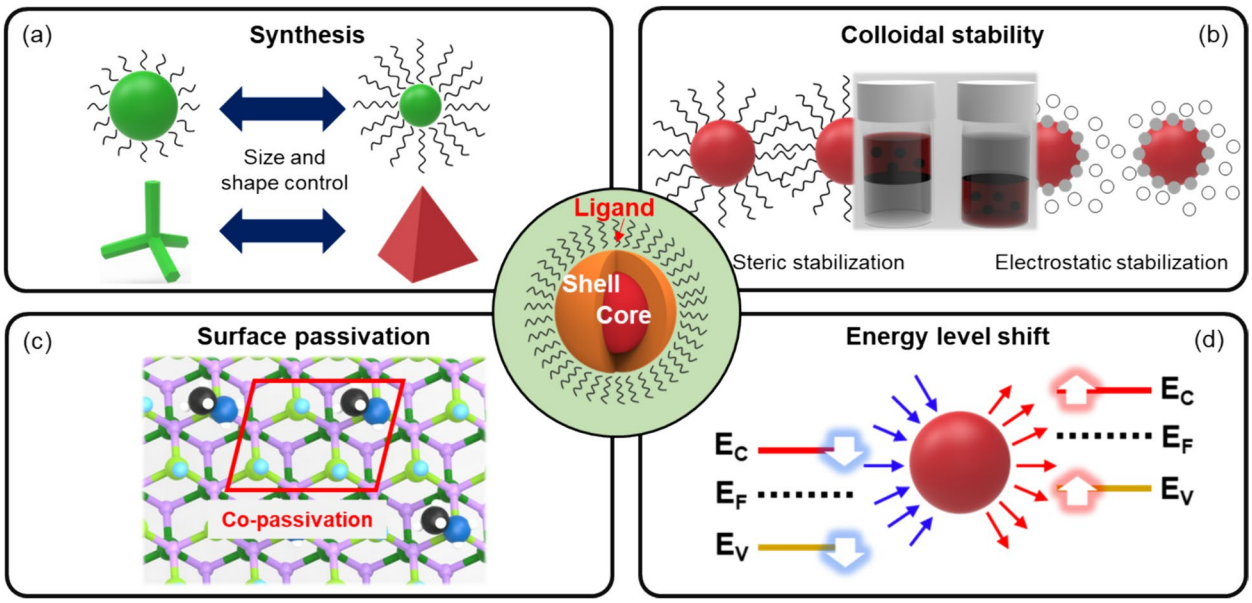

Fig. 1 Role of ligands in semiconductor NCs. **a** Synthesis (size and shape control), **b** colloidal stability, **c** surface passivation, and **d** energy-level control

The facet-selective binding of ligands hinders the growth of crystals along the < 111 > direction, leading to the formation of (111) facet-terminated octahedrons. On the other hand, when PbS NCs were synthesized by adding oleic acid with DDT (1:1 volume ratio), the binding to the (111) facet became weaker and crystal growth occurred preferentially along the < 111 > direction, resulting in the formation of (100) facet-terminated cube [17, 18]. Similarly, the structure of the InAs NCs can be controlled through ligand engineering. Manna et al. synthesized tetrahedral InAs NCs using indium chloride, zinc chloride, tris(dimethylamino)arsine precursor, alane *N,N*-dimethylethylamine complex solution, and oleylamine ligands [19]. Here, oleylamine binds to the (111) facet of the InAs NCs and strongly stabilizes this facet, and the influence of $ZnCl_2$ precursor leads to the formation of tetrahedral structures in the InAs NCs [20]. However, when bulkier amine ligands, such as trioctylamine, were added during the growth of InAs NCs, the steric influence of these ligands (which only allows weak binding of ligands at the edges and corners of the NCs) led to the production of InAs NCs with different structures. InAs in tetrapod structures were formed, particularly when a 4:1 molar mixture of trioctylamine and oleylamine was used. Under such conditions, the steric hindrance of trioctylamine affected the density of oleylamine bound to the (111) facet, leading to the growth of arms along the < 111 > direction. This led to the formation of tetrapod InAs NCs entirely in a zinc-blende structure, different from Cd-based II–VI tetrapod NCs containing a zinc-blende core attached with four wurtzite arms [21]. When carboxylic acid, trioctylphosphine, or dioctylamine ligands were introduced instead of trioctylamine, the size and shape of the NCs could not be precisely controlled, and the size distribution of the resulting NCs was poor. There were also some studies that synthesized nanorods or nanoplatelet NCs by gradually adjusting their shape by controlling the ligands [22–24].

The choice of ligands can also affect the reaction conditions. When fatty acids were used as the ligands in the synthesis of InP NCs, the reaction temperature is generally above 250 °C in noncoordinating solvents, which is a high temperature condition that can produce undesirable In_2O_3 by the hydrolysis of In carboxylate [25]. Consequently, careful degassing is required for the synthesis of InP to avoid oxidation. Peng et al. found that adding fatty amines, which are common activation reagents as well as good ligands to improve the emission properties of II–VI NCs, during the synthesis of InP NCs could significantly lower the reaction temperature below 190 °C [26]. This enabled the production of InP NCs without tedious degassing during the synthesis process. Bawendi et al. found that the addition of amines (octylamine) during the synthesis of InP slowed the abrupt consumption of phosphine precursors, that is, tris(trimethylsilyl)phosphine, during the nucleation step, which allowed the stable growth of the crystal without depletion during later stages [27].

Influence of Ligands on the Colloidal Stability of Semiconductor NCs

NCs can be dispersed in solvents, and the resulting colloidal stabilities of the NCs vary depending on the interactions

between the ligands and solvents. Two different mechanisms can be applied to stabilize the colloids: steric and electrostatic mechanisms (Fig. 1b) [9]. Steric stabilization plays a more critical role, especially when nonpolar organic ligands, typically composed of hydrocarbon chains, are introduced during synthesis. When NCs capped with such ligands are immersed in a good solvent (for the ligands), the favorable interaction between the solvent and hydrocarbon chains causes the hydrocarbon chains to stretch out rather than contract. The associated entropic repulsion of the ligands facilitates a stable dispersion of the NCs. Furthermore, the solvent–ligand interactions also depend on the packing structure of the hydrocarbon chains, which in turn affects the colloidal stability of the NCs. Unsaturated bent-chain ligands (such as 4-ethyloctanoic acid or 2-hexyldecanoic acid) pack the NCs less efficiently than saturated straight-chain ligands (such as stearic acid) [28]. Consequently, solvents can intercalate more easily with NC surfaces covered with unsaturated bent-chain ligands, leading to the formation of NCs with higher colloidal stability, consistent with the experimental finding that using oleic acids yields more stable NCs than using stearic acids as the ligands. This indicates that more entropic ligands that pack less efficiently can further improve the colloidal stability of the NCs. Moreover, these ensure the stable dispersion of NCs in solvents, even at much higher concentrations. Despite the improvements in colloidal stability, the density of the unsaturated dangling bonds on the NC surface (and the associated trap states) can be higher as the ligands are more loosely packed; however, this aspect has not been researched extensively. Meanwhile, controlling the density of ligands can also form excellent and diversely shaped nanorod NC monolayers at the air/solution interface during the dip-coating process [29, 30].

Electrostatic stabilization of NCs can be achieved when charged species are adsorbed onto NC surfaces or if the surface ligands are charged. The dispersion of the NCs s balanced by oppositely charged counterions, located in the diffuse regions around the NCs in a good solvent. Good solvents, such as formamide, generally have a high dielectric constant, facilitating the effective screening of electrostatic attractions. In these solvents, the entropic penalty associated with counterion condensation in diffusion double layers prevents charge-stabilized NC surfaces from approaching each other. However, poor solvents with low dielectric constants, such as toluene, induce the collapse of diffuse counterions. In such solvents, the electrostatic repulsion between the NCs is insufficient to overcome the attractive forces, leading to aggregation. Based on electrostatic stabilization, NCs with suitably charged ligands can be dispersed in environmentally friendly polar solvents (e.g., ethanol, propylene glycol methyl ether acetate, and isopropyl alcohol), which are widely accepted in industry. It was reported that InP/$ZnSe_xS_{1-x}$ NCs, when partially passivated with mono-2-(methacryloyloxy)ethyl succinate ligands featuring carboxylate head groups and acrylate tail groups, can be effectively dispersed in green polar solvents such as diethylene glycol monoethyl ether acetate and propylene glycol methyl ether acetate [31]. These NCs preserved their photophysical properties and were successfully implemented in processing methods like inkjet printing and even to photolithography processes, particularly when combined with photocrosslinkable resins.

Passivation of NC Surface with Ligands

Ligands on the NC surface can influence the optical and electrical characteristics of the NCs. The surface atoms of NCs, if not bound with ligands, form dangling bonds, which contribute to the formation of electronic states within the NC bandgap [32]. These states can behave as trap states for carriers, disturbing the charge transport of NCs or quenching excitons and the associated luminescence characteristics. Although optical stability or fluorescence quenching can be improved by controlling the shell thickness of NCs or coating them with materials such as silica, ligands have a more direct effect [33, 34]. When ligands bind to the surface atoms of NCs, the resulting set of molecular orbitals with bonding and antibonding characteristics, formed between the ligands and surface atoms, can shift outward from the bandgap of the NCs. Therefore, the trap states and quenching sites associated with the dangling bonds become passivated.

For complete passivation of the dangling bonds, the required ratio between the surface atoms and ligands can vary depending on the bonding characteristics of the NC surface atoms and their arrangement, according to the atomic ligand model developed by Kim et al. [35]. For example, Cd atoms in CdSe NCs possess two valence electrons that should be shared with four neighboring Se atoms, contributing six electrons. If a dangling bond exists, each dangling bond on Cd atom exhibits electronic characteristics associated with 1.5 (=6/4) deficient electrons. For the (111) plane of zinc-blende CdSe NCs, each Cd surface atom (having one dangling bond) has 1.5 deficient electrons. Complete passivation occurs when each surface atom receives 1.5 electrons, or alternatively, when two surface atoms receive 3 electrons from the ligand. Hence, two Cd surface atoms on the (111) plane should be passivated by one monovalent X-type ligand (such as halide ions) and one L-type ligand (such as amine ligands donating two electrons) [36, 37]. Similarly, In atoms in III–V NCs like InP have three valence electrons, leading to 1.25 (=5/4) deficient electrons per dangling bond. On the (111) plane of zinc-blende InP NCs, each In surface atom also possesses one dangling bond, displaying 1.25 deficient electrons per atom. When four In surface atoms form a unit, they require a total of 5 ($=1.25\times4$) additional electrons for

complete passivation, which can be achieved via a 3:1 co-passivation of X-type and L-type ligands (Fig. 1c).

Energy Level Control by Ligand Engineering

Surface ligands can shift the energy levels of NCs. Specifically, the electric dipoles formed by the ligands influence the energy levels of the NCs depending on the orientation and magnitude of the dipole. If the dipole orientation points toward the NCs, the energy levels shift downward, and vice versa for the opposite case (Fig. 1d). The orientation and magnitude of these dipoles are determined by the combination of (i) the interfacial dipole between the surface atom and ligand and (ii) the intrinsic dipole of the ligand itself. The interfacial dipole varies depending on the local characteristics of the surface atoms and binding modes of the ligands, whereas the intrinsic dipole of the ligands depends on their chemical structure. Bulovic et al. demonstrated that the energy levels of PbS NCs vary with the use of 12 different ligands [38]. Even among chemically similar ligands such as 1,2-ethanedithiol (EDT), 1,2-benzenedithiol (1,2-BDT), and 1,3-benzenedithiol (1,3-BDT), shifts of more than 0.2 eV were observed in the valence band maximum (VBM), leading to different photocurrent generations in photovoltaic devices. Similarly, the ligand engineering of InAs NCs enables the tuning of the energy levels of the material [39]. These studies confirmed that the trap states and energy levels of NCs can be controlled through ligand engineering alone. Moreover, they suggest that ligand engineering can play a key role in improving the performance of NC-based optoelectronic devices, such as LEDs, PVs, and photodiodes.

Application of Ligand Engineered NCs

Thin-Film Transistors

TFTs are electrical devices in which conduction through a semiconductor channel is modulated via capacitive control of charge density through a gate bias. The electrical characteristics of NC-based thin-film transistors depend on the charge transport between the NCs. Because charge transport through NC films is based on carrier hopping between neighboring NCs, increasing the strength of the electronic coupling between neighboring NCs is critical for enhancing conduction through the TFT channels [40]. Because the ligands employed during the synthesis of NCs are typically long insulating molecules, they serve as blocking units that hamper the strong coupling between NCs. Consequently, efforts have been made to replace these ligands (either before forming the transistor channel or after forming the transistor channel) with short molecules or small inorganic ions and even to remove these ligands before coating the channel layer. In this subsection, we review various ligand engineering performed on NCs, which have been extensively studied in the context of NC-based TFTs.

In atoms on the InAs NCs surface bound to soft As atoms are soft Lewis acids, unlike free In^{3+} ions, which are hard Lewis acids [41]. Consequently, soft Lewis base ligands (such as thiols) bind favorably to the InAs NCs. In this context, EDT ligands are commonly used as exchange ligands for InAs NCs. EDT ligand exchange has been performed mostly in solid phase, where predeposited NC thin films in solid state are exposed to or dipped in a solution containing EDT [42–47]. Because the EDT ligands are shorter than the original ligands bound to the as-synthesized InAs NCs, the interparticle distance for the InAs NC films treated with EDT is shorter than that of the original films. The resulting enhancement in electronic coupling leads to effective charge transport between the NCs and across the entire NC film. This yields an electron mobility as high as 0.53 cm^2/V s [45]. Other soft Lewis base ligands (including sulfur ions and halides such as bromide, iodide, and chloride ions), which can shorten the interparticle distance between InAs NCs compared with EDT, can also be used in solid-state exchange methods [46]. Recently, an EDT exchange process was conducted with photopatterned InAs NC films, obtained using a photochemical crosslinking agent (light-induced ligand crosslinker (LiXer)) that can form chemical bonds between the ligands of neighboring NCs under UV irradiation. By combining the photopatterning process and ligand-exchange step, Kang et al. demonstrated the fabrication of InAs NC-based complementary logic circuits (Fig. 2) [46].

Even though solid-state ligand exchange for InAs NCs films can be conducted simply, this method inherently suffers from crack formation in the NC films after the exchange process owing to the reduced interparticle distance [40]. This requires an exchange process in the solution phase prior to the deposition of materials on the thin films. Talapin et al. demonstrated a method for introducing molecular chalcogenide complex (MCC) ligands onto InAs NCs using a solution-state exchange method [48, 49]. An InAs NC solution in hexane was added to an MCC solution in hydrazine at a molar ratio of 1:1. After stirring the solution, the ligands of the InAs NCs were replaced with the MCC ligands, and the MCC-capped InAs NCs were dispersed in hydrazine (Fig. 3a). TFTs based on $Cu_7S_4^-$-capped InAs NCs exhibited high electron mobilities exceeding 10 cm^2/V s (Fig. 3c and d), which is by far the highest value reported for InAs NC TFTs. The same research group demonstrated that inorganic halides, pseudohalides, and halometallate ligands could be introduced using the same exchange method. TFTs based on pseudohalide ligand (N_3^-) treated-InAs NCs exhibited a mobility of 0.16 cm^2/V s [50].

Alivisatos et al. demonstrated a surface passivation method for In-based NCs in solution phase by fluorination

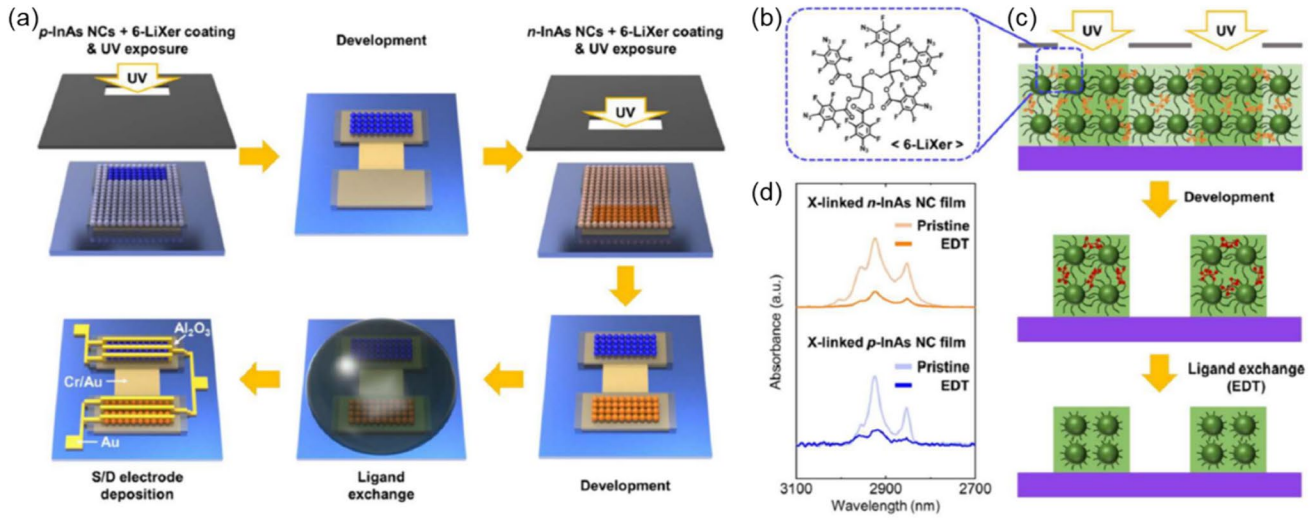

Fig. 2 **a** Schematic description of the fabrication of a complementary logic circuit based on InAs NCs. **b** Chemical structure of 6-LiXer. **c** Schematic description of the patterning and ligand exchange processes for InAs NC films. **d** Fourier transform infrared (FTIR) spectra before and after exchanging the ligands of the InAs NCs films. Reprinted with permission from Ref. [46]. Copyright 2023, American Association for the Advancement of Science

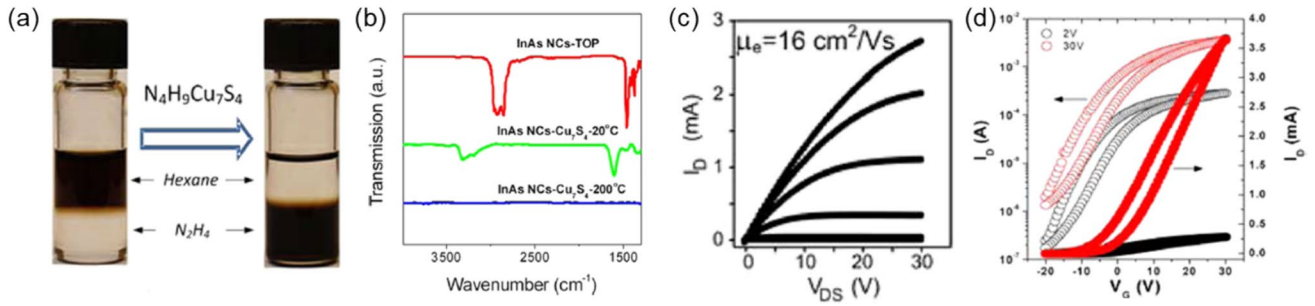

Fig. 3 **a** Photographs showing the phase transfer of NCs from a hexane phase to a hydrazine phase, including MCC ligands. **b** FTIR spectra before and after exchanging ligands and after heating of the InAs NC films. **c** Output and **d** transfer characteristics of transistors based on $Cu_7S_4^-$-capped InAs NCs. Reprinted with permission from Ref. [48]. Copyright 2012, American Chemical Society

rather than by replacing long organic ligands with other ligands [47]. They confirmed that through a low-concentration hydrofluoric acid (HF) treatment, fluoride ions directly passivated the indium dangling bonds of InP NCs in the form of atomic ligands and thereby enhanced the luminescence. To verify that fluoride effectively passivates dangling In bonds, they employed InAs NCs as model systems and treated the InAs NCs with HF (Fig. 4a). The photoluminescence quantum yield (PLQY) increased from 1.5 to 11% after HF treatment, indicating that the InAs NCs were reactive to fluorine (Fig. 4b). Because the HF treatment removes long organic ligands and surface traps, fluorinated InAs NCs were applied to the TFTs. Compared to the EDT-treated InAs NCs, which exhibited a quasi-linear output curve and transfer curve that was not sufficiently turned off owing to the high carrier concentration (Fig. 4c) [51], the fluorinated InAs NCs exhibited a clearly saturated output curve and transfer curve with a sufficiently low off-state current (Fig. 4d). The linear mobility of the fluorinated InAs NC films (2.8×10^{-4} cm^2/V s) was one order of magnitude higher than that of its EDT-treated InAs NCs counterpart (2.3×10^{-5} cm^2/V s). In terms of photoresponse, the EDT-treated InAs NCs exhibited a much slower on/off photoresponse than the fluorinated InAs NCs. The photocurrent did not saturate even after 250 s of illumination, and the dark current did not reach the off state. In contrast, fluorinated InAs NCs demonstrated a clearly saturated photo-/dark-current and fast photoresponse owing to the effective passivation of trap states.

Among the ligand engineering methods mentioned above, MCC-capped InAs NCs exhibited mobilities exceeding 1 cm^2/V s. However, new ligand engineering methods that

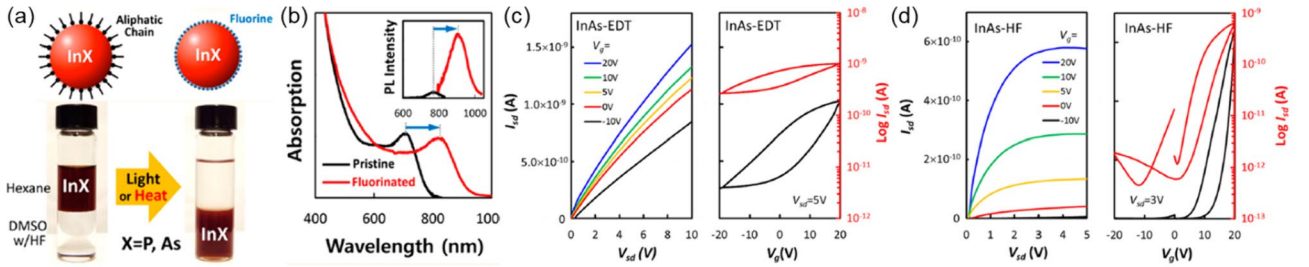

Fig. 4 **a** Photograph showing the phase transfer of NCs from a hexane phase to a dimethyl sulfoxide phase, including HF. **b** Optical absorption and PL spectra of pristine and HF-treated InAs NCs. Output and transfer characteristics of transistors based on **c** EDT-treated and **d** fluorinated InAs NCs. Reprinted with permission from Ref. [47]. Copyright 2018, American Chemical Society

lead to high mobility are needed because the use of MCC ligands involves reactive and corrosive chemicals. Kagan et al. demonstrated high-mobility TFTs based on InAs NCs using a hybrid ligand exchange method that combined solid- and solution-state exchange methods [52]. In this method, Na_2S ligands were used because sulfide can serve as an effective compact ligand on InAs NC surfaces. Thin films were then formed with the InAs NC films via a solution-state exchange method. Subsequently, a solid-state exchange method was performed (NaN_3 ligands were used instead of Na_2S ligands; see below), and this resulted in TFTs with higher mobility compared to those based on InAs NC films processed by each method alone. While the hybrid ligand-exchange method successfully boosted the electronic coupling between InAs NCs, the excessive incorporation of sulfur led to an increase in the electron concentration and yielded TFTs with a high off-state. To prevent this, NaN_3 ligands were used instead of Na_2S during the solid-state exchange step. The resulting film yielded not only a superior gate modulation with low off state currents but also a higher mobility (5.46 ± 0.37 cm^2/V s) compared to NC films exchanged with Na_2S ligands in solid state (4.03 ± 0.26 cm^2/V s). Both Na_2S- and NaN_3-treated InAs NCs exhibited positive photoconductivity when illuminated by light energies larger than their bandgaps. This is consistent with the prediction that carrier trapping can be suppressed by increasing the amount of sulfur introduced via ligand exchange.

The synthetic methods developed for InP NCs thus far involve the formation of a core/shell structure for visible-light emission. Although shelling the InP core can enhance the luminescence characteristics of NCs, the shell material typically has a larger band gap than the core; therefore, it often acts as an energy barrier, preventing efficient charge transport between NCs. Consequently, InP NCs are more widely utilized for LEDs, with limited research focusing on TFT applications. Talapin et al. demonstrated that InP NCs could be replaced with MCC ligands through solution-state exchange methods [48]. However, as mentioned earlier, the MCC ligand-exchange method requires the use of reactive and corrosive chemicals; therefore, alternative ligand-engineering methods are being sought. The hybrid ligand-exchange method, which was introduced for InAs NCs by Kagan et al., has also been applied to tetrahedral InP NCs [53]. The NCs in the solution were treated with nitrosyl tetrafluoroborate ($NOBF_4$) to remove surface oxides. Solid-state ligand exchange was performed using Na_2S, Na_2Se, NaN_3, NH_4Cl, and EDT ligands. The Na_2S and Na_2Se ligands exhibited higher exchange rates than the other ligands, resulting in a further reduction in the distance between the NCs. Between the two, thin films of Na_2S-treated InP NCs showed higher electron mobility (3.2×10^{-2} cm^2/V s), while those of Na_2Se-treated InP NCs showed poorer current modulation due to over-doping (1.5×10^{-3} cm^2/V s). To enhance the degree of ligand exchange, InP NCs were treated with Na_2S ligands in solution, and NaN_3 ligands were then introduced through solid-state ligand exchange. This prevented over-doping due to the excess introduction of sulfur ligands (Fig. 5). The results obtained for different InAs or InP NCs films with different ligand treatments are summarized in Table 1.

Photovoltaics and Photodetectors

PV devices and photodetectors convert light energy into electrical energy and signals, respectively. This requires an adequately large volume of NCs to absorb sufficient light; therefore, the NC films employed in these devices are typically thicker than those used in TFTs or LEDs. Because the charge carriers photogenerated within such thick NC films must be transported efficiently to the electrodes before recombination, acquiring NC films with excellent transport characteristics is as important as obtaining NC films in TFTs. This can be achieved by replacing the long organic ligands with short ligands.

Jeong et al. developed a chemical treatment based on $NOBF_4$ that removes not only the long organic ligands on InAs NCs, but also the undesirable oxides on the surface that are inevitably formed during the synthesis [39]. This was

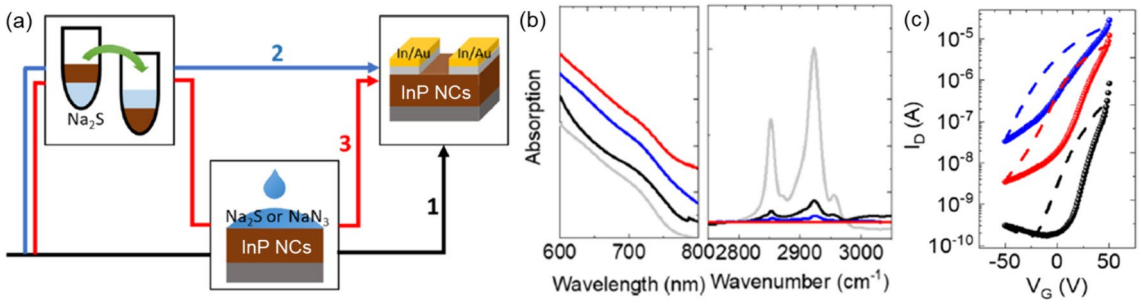

Fig. 5 **a** Schematic description of the ligand exchange pathways of InP NCs for TFT applications. **b** UV–Vis and FTIR spectra of the as-synthesized (gray) InP NC films, after Na_2S ligand exchange in solid-state (black), Na_2S ligand exchange in solution-state (blue), and hybrid Na_2S and NaN_3 (red) ligand exchange in solution- and solid-states. **c** Transfer characteristics of TFTs based on InP NCs after Na_2S ligand exchange in solid-state (black), Na_2S ligand exchange in solution-state (blue), and hybrid ligand exchange (red). Reprinted with permission from Ref. [53]. Copyright 2022, American Chemical Society

Table 1 Summary of the carrier type, size, exchanged ligands, ligand exchange methods, and mobility of TFTs based on InAs and InP NCs treated with various ligands

Nanocrystal	Carrier type	Size (nm)	Exchanged ligands	Ligand exchange method	Mobility (cm^2/V s)	References
InAs	*n*-type	N/A	EDT	Solid-state	N/A	[42]
InAs (Cd-doped)	*p*-type	N/A	EDT	Solid-state	N/A	[42]
InAs	*n*-type	5.1	EDT	Solid-state	2.3×10^{-5} (linear)	[47]
InAs	*n*-type	4.5	EDT	Solid-state	0.08 (linear), 0.07 (saturation)	[43]
InAs (Cu-doped)	*n*-type	4.5	EDT	Solid-state	0.18 (linear), 0.15 (saturation)	[43]
InAs	*n*-type	4.68	EDT	Solid-state	0.31 (linear)	[44]
InAs (Cd-doped)	*p*-type	4.77	EDT	Solid-state	1.5×10^{-3} (linear)	[44]
InAs	*n*-type	5	EDT	Solid-state	0.53 (linear)	[45]
InAs (Zn-doped)	*p*-type	5	EDT	Solid-state	1.2×10^{-5} (linear)	[45]
InAs	*n*-type	4.6	EDT	Solid-state	3.9×10^{-3} (linear), 3.9×10^{-3} (saturation)	[46]
InAs (Zn-doped)	*p*-type	3.5	EDT	Solid-state	2.3×10^{-3} (linear), 3.3×10^{-3} (saturation)	[46]
InAs	*n*-type	4.6	$Cu_7S_4^-$	Solution-state	16.0 (linear), 14.8 (saturation)	[48]
InAs	*n*-type	N/A	N_3^-	Solution-state	0.16 (linear)	[50]
InAs	*n*-type	5.1	Fluoride ion	Solution-state with HF treatment	2.8×10^{-4} (linear)	[47]
InAs	*n*-type	N/A	S^{2-}	Solid-state	3.2×10^{-3} (N/A)	[52]
InAs	*n*-type	N/A	S^{2-}	Solution-state	0.25 (N/A)	[52]
InAs	*n*-type	N/A	S^{2-}	Hybrid (solid + solution)	4.03 (N/A)	[52]
InAs	*n*-type	N/A	$S^{2-}+N_3^-$	Hybrid (solid + solution)	5.46 (N/A)	[52]
InP	*n*-type	4.0	$Sn_2S_6^{4-}$	Solution-state	0.09 (linear), 0.05 (saturation)	[48]
InP (tetrahedral)	*n*-type	6.5 (height)	Se^{2-}	Solid-state	1.5×10^{-3} (saturation)	[53]
InP (tetrahedral)	*n*-type	6.5 (height)	S^{2-}	Solid-state	3.2×10^{-2} (saturation)	[53]
InP (tetrahedral)	*n*-type	6.5 (height)	S^2	Solution-state	0.27 (saturation)	[53]
InP (tetrahedral)	*n*-type	6.5 (height)	$S^{2-}+N_3^-$	Hybrid (solid + solution)	0.21 (saturation)	[53]

done for InAs NCs in solution state by adding $NOBF_4$ dissolved in N, N-dimethylformamide (DMF), which resulted in InAs NCs passivated by BF_4^- ions that were well-dispersed in the DMF [54]. X-ray photoelectron spectroscopy (XPS) and FTIR analyses confirmed that As_2O_3 and organic ligands on the NC surface were completely removed after the $NOBF_4$ treatment (Fig. 6b and d). However, the PL intensity of the $NOBF_4$-treated InAs NCs was effectively quenched because of the imperfect passivation of the InAs NCs, which indicated the presence of numerous surface defects. When $NOBF_4$-treated InAs NCs were mixed with a solvent in which short or halide ligands were dispersed,

the ligands re-passivated the surface (Fig. 6a and e), and the PL intensity was recovered (Fig. 6f). InAs NCs passivated by 3-mercaptopropionic acid (MPA) ligands exhibited the highest mobility, and they were utilized in *p–n* junction photovoltaics with *p*-type PbS NCs, showing a power conversion efficiency (PCE) of 7.92% (Fig. 6g and h).

Although $NOBF_4$ treatment can effectively remove native ligands and unwanted oxide layers, it requires the use of toxic solvents, such as DMF, which can potentially limit the manufacturing process. In addition, when functional ligands having low reactivity (such as ethanethiol) are applied to replace the original ligands along with the $NOBF_4$ treatment, the method often results in InAs NCs with residual BF_4^- and incomplete surface passivation. Baek et al. presented an intermediate phase transfer (IPT) method, in which the ligand was successfully exchanged while being dispersed in green solvents such as 2-methyltetrahydrofuran (2-meTHF) and 2-methylanisole (2-MA) (Fig. 7a) [55]. IPT was enabled by pretreating the NCs with short benzoic acids, which partially exchanged the original long carboxylic acid ligands. Because of the highly polarizable aromatic ring of the ligands, the resulting NCs containing benzoic acid ligands were well dispersed, even in weakly polar solvents [56, 57]. Subsequently, the remaining long carboxylic acid ligands were readily replaced with short ligands with thiol groups (e.g., ethanethiol), because the resulting NCs partially exchanged with short benzoic acid ligands exhibited small steric hindrance [58]. Through IPT, the InAs NC surface was completely passivated with benzoic acid and ethanethiol ligands. In addition, the successful transfer of QDs from a nonpolar solvent phase (octane) to a weakly polar solvent phase (2-meTHF) was demonstrated. Even after the introduction of thiol ligands, the benzoic acid ligands remained on the NC surface, providing sufficient surface passivation and colloidal stability. Unlike the NC films prepared using other ligand-exchange methods, the NC films prepared using the IPT method were uniform with no apparent cracks or pinholes. This led to enhanced near infrared (NIR) photodetector characteristics, achieving an external quantum efficiency (EQE) of 292% and rise/fall times of 12.4/36.1 ns (Fig. 7b and c).

The as-synthesized InAs NCs are typically passivated by oleic acid ligands, and they exhibit In-rich stoichiometry. This off-stoichiometry can lead to the formation of intragap states, which deteriorate charge transport, promote nonradiative recombination, and prevent efficient optoelectronic operation [59, 60]. To address this issue, Sargent et al. replaced the oleic acid ligands with 2-mercaptoethanol (ME) ligands using a solution-state exchange method [61]. An XPS analysis confirmed that the As/In ratio increased after ligand exchange, indicating that the ME ligands replaced the In metal-oleic acid ligands in pairs, resulting in an overall decrease in the effective NC size. Additionally, they reported the presence of an As-S peak, suggesting the formation of covalent bonds between the surface atoms and thiol ligands, which are not typically observed for ionic II–VI and IV–VI NCs. ME-capped InAs NCs were used as the active layer in photodiode detectors. The devices exhibited an EQE of 36% at a reverse bias of 1 V, and the photoresponse time was four times shorter than those of the PbS NC devices.

The same research group introduced $InBr_3$ ligands that can passivate both In and As sites [62]. For the $InBr_3$

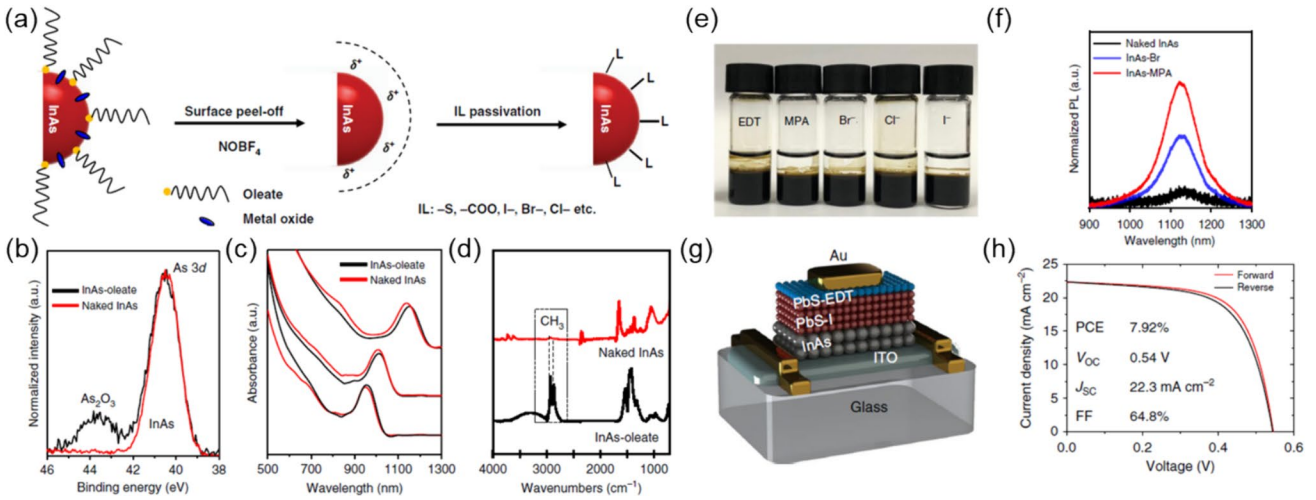

Fig. 6 **a** Schematic description of the two-step surface modification of InAs NCs. **b** XPS spectra, **c** UV–Vis spectra, and **d** FTIR spectra of InAs NCs before (black lines) and after (red lines) $NOBF_4$ treatment. **e** Photograph of InAs NCs after surface reconstruction with various ligands. **f** PL spectra of $NOBF_4$-treated (black line), Br-treated (blue line), and MPA-treated (red line) InAs NCs. **g** Schematic architecture of *p–n* junction photovoltaics using *n*-type InAs NCs. **h** Newport certification of the photovoltaics: current density–voltage (*J–V*) characteristics. Reprinted with permission from Ref. [39]. Copyright 2018, Springer Nature

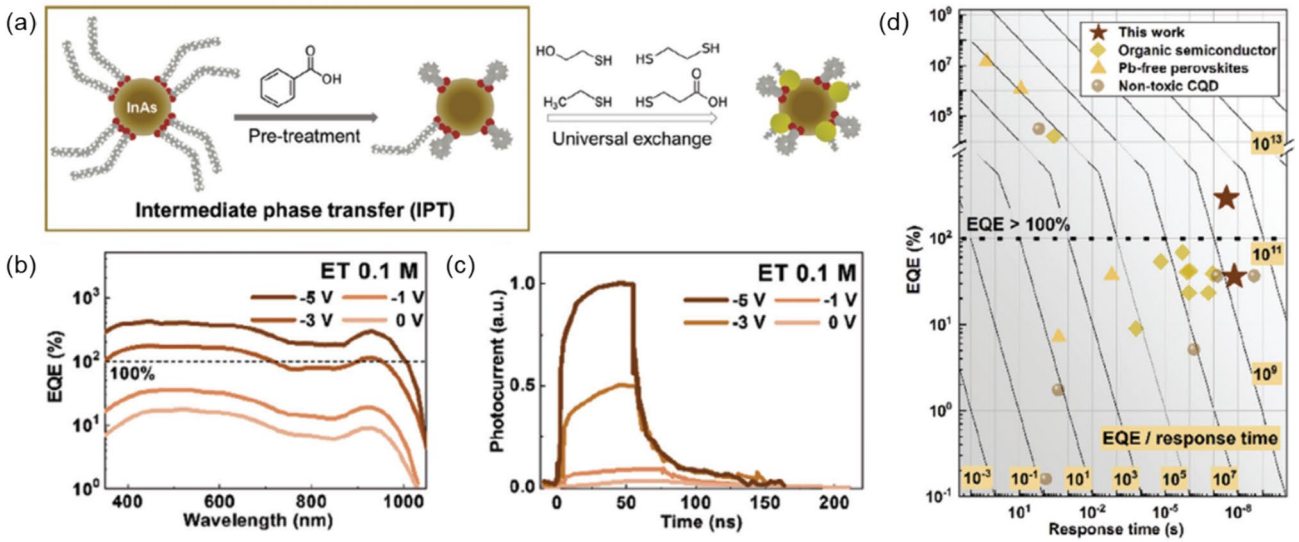

Fig. 7 **a** Schematic description of a ligand exchange method using the IPT method. **b** EQE and **c** transient photoresponse of IPT-treated InAs NC photodiodes. **d** Summary of EQE versus response (fall) time of the solution-processed NIR photodetectors based on different materials including non-toxic NCs, Pb-free perovskites, organic semiconductors, and ref [55] work. The grid line indicates EQE/response time used as a figure of merit (FOM). Reprinted with permission from Ref. [55]. Copyright 2024, Wiley–VCH GmbH

ligand, Br^- passivates the In dangling bonds and $InBr_2^+$ passivates As dangling bonds. $InBr_3$-treated InAs NCs showed a mobility of 0.04 cm^2/V s. Photodiodes based on $InBr_3$-treated InAs NCs showed an EQE of 30% at 0 V and a specific detectivity of 10^{11} cm $Hz^{1/2}/W$. A fall time of 2 ns, which is the fastest recovery rate among NC photodiodes reported to date, was achieved owing to the low permittivity and good carrier transport. Later, this group introduced a methylammonium acetate (MaAc) ligand in addition to the $InBr_3$ ligand (Fig. 8a) [63]. The binding energy of the acetate group on the InAs (111) facets was higher than that of Br; therefore, the MaAc ligands bound more strongly to the InAs NCs. Dark current analyses of hole- and electron-only devices confirmed that mobility was almost constant, while the electron and hole trap densities decreased by 80 and 50%, respectively, after MaAc ligand treatment. The MaAc-treated InAs NC photodiodes showed an EQE of 37% and a detectivity of 1.9×10^{11} Jones (Fig. 8c and d).

Despite these co-passivation strategies, InAs NC-based devices still exhibited a high dark current and low EQE

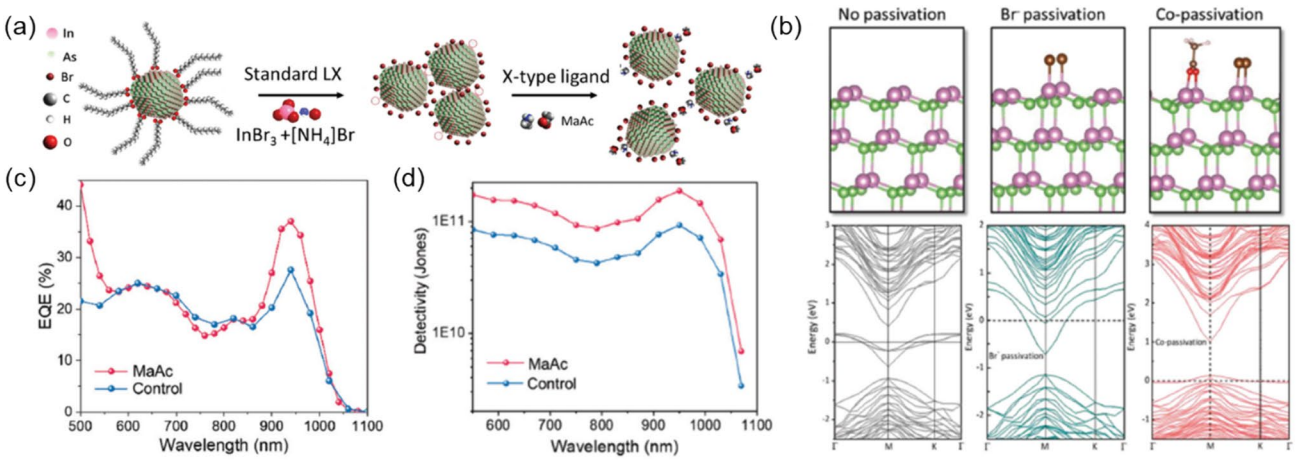

Fig. 8 **a** Schematic description of ligand exchange with the addition of MaAc ligand. **b** Discrete Fourier transform (DFT) simulation; side views of ball-and-stick models of InAs (111) facet with naked, pure Br^- passivation, and co-passivation with Br^- and acetate; and their respective band structures near Fermi energy level (dash line). **c** EQE and **d** detectivity of InAs NC photodetectors. Reprinted with permission from Ref. [63]. Copyright 2023, Wiley–VCH GmbH

compared with PbS NC devices. Oh et al. examined the interactions between metal halide ligands and InAs NC surfaces to fabricate high-performance InAs NC-based IR photodetectors [64]. Based on the hard-soft acid–base theory, three types of metal halide ligands (CdX_2, InX_3, and SnX_2; X = Cl, Br, or I) were introduced. Among these ligands, the hard-type SnX_2 ligand exhibited a higher affinity for hard-type surface As atoms than the other soft- (CdX_2) and intermediate-type (InX_3) ligands. Regardless of the metal type, iodides exhibited the lowest degree of ligand exchange. Overall, the $SnCl_2$ and $SnBr_2$ ligands exhibited the highest degrees of ligand exchange. The $SnBr_2$-treated InAs NC film exhibited a higher mobility of 1.02×10^{-3} cm^2/V s and shorter carrier lifetime of 1262 ± 400 ps, and the $SnBr_2$-treated InAs NC-based photodetectors achieved an EQE of 43.1% and a responsivity of 0.36 A/W.

Hens et al. demonstrated the first short wavelength infrared (SWIR)-sensitive photodiodes based on NCs without toxic elements (such as PbS and HgTe NCs), using tetrahedral In(As, P) NCs [65]. Tetrahedral In(As, P) NCs were originally co-passivated by Cl^- and oleylamine ligands. By exposing NCs to carboxylic acids or thiols that can be deprotonated, one equivalent of Cl^- and oleylamine ligands could be removed from the surface by forming oleylammonium chloride, resulting in a surface passivated with carboxylates or thiolates [66, 67]. Thus, the ligands of the tetrahedral In(As, P) NCs were exchanged with a mixture of 3-mercapto-1,2-propanediol (MPD) and *n*-butylamine. Here, the MPD ligands were deprotonated leading to the removal of the Cl^- and oleylamine ligands on the NC surface. *n*-butylamine promoted the displacement of Cl^- through butylammonium chloride formation, and it was directly involved in the ligand exchange with oleylamine ligands. The resulting *n*-type tetrahedral In(As, P) NCs with short MPD and butylamine ligands formed a heterojunction with the *p*-type NiO and served as a photoactive layer for the photodiode. These stacks exhibited rectified current–voltage behaviors in dark, and the photocurrents increased proportionally with the light intensity. Spectral EQE plot tracks the NC absorbance spectrum to produce photosensitive films up to 1400 nm, achieving an internal quantum efficiency (IQE) of up to 46%.

Seong et al. developed a hybrid phototransistor by stacking InAs NCs onto a high-mobility zinc oxynitride (ZnON) [68]. After the formation of an InAs NC thin film on ZnON, ME ligands were introduced via solid-state exchange. Additionally, a thin film of $InCl_3$-treated InAs NCs was placed on top of the ME-treated InAs NCs, which formed a layer with a well-aligned band structure suitable for improved spatial separation of photogenerated electrons and holes. Owing to the combination of the excellent light-absorbing properties of InAs NCs, high mobility of ZnON, and well-aligned energy structure, the hybrid phototransistor exhibited a responsivity and detectivity of over 10^5 A/W and 10^{16} Jones, respectively. Device characteristics of photodetectors based on different InAs NCs films with different ligand treatments are summarized in Table 2.

Compared to InAs NCs, the reports on InP NCs for PV or photodetector applications are limited because InP NCs are mainly active in the visible range. Houtepen et al. fabricated a PV device using highly photoconductive InP NC films, obtained via treatment with EDT, Na_2S, or $(NH_4)_2S$ [69]. They used time-resolved microwave conductivity (TRMC) to measure the mobility and lifetime of the photogenerated charge carriers in InP NC films. While both the mobility and lifetime of the $(NH_4)_2S$-capped InP NCs were similar to those of the PbS NCs, traps capturing the charge carriers on

Table 2 Summary of the first exciton peak wavelength, exchanged ligands, ligand exchange method, EQE, responsivity, and detectivity of photodetectors based on InAs NCs treated with various ligands

Nanocrystal (device type)	Wavelength (nm)	Exchanged ligands	Ligand exchange method	EQE (%) [bias]	Responsivity (A/W)	Detectivity (Jones)	References
InAs (photodiode)	920	Benzoic acid + ethanethiol	IPT method + solution-state	292 [− 5 V]	2.19	1.1×10^{11}	[55]
InAs (photodiode)	930	ME	Solution-state	36 [− 1 V]	0.27	1.6×10^{11}	[61]
InAs (photodiode)	940	$InBr_2^+ + Br^-$	Solution-state	30 [0 V]	0.22	1.0×10^{11}	[62]
InAs (photodiode)	950	$InBr_2^+ + Br^- + MaAc$	Solution-state	37 [0 V]	0.283	1.9×10^{11}	[63]
InAs (photodiode)	1020	$SnBr^+ + Br^-$	Solid-state	43.1 [− 1 V]	0.36	1.62×10^{10}	[64]
In(As, P) (photodiode)	1140	MPD + *n*-butylamine	Solution-state	5 [− 4 V]	0.031	1.1×10^{10}	[65]
InAs (phototransistor)	1020	ME, $InCl_2^+ + Cl^-$	Solid-state	1.58×10^7 [20 V]	1.15×10^5	5.32×10^{16}	[68]

a ~ 10 ns time scale, which contributed to a decrease in photoconductivity, were observed. Trap filling was not observed in the $(NH_4)_2S$-treated InP NCs containing Zn (which was introduced during the synthesis process), suggesting that Zn passivated the traps. Based on the $(NH_4)_2S$-treated InP and $(NH_4)_2S$-treated InZnP NCs, PV devices with PCEs of 0.65 and 1.2%, respectively, were demonstrated. The characteristics of PV devices based on various InAs and InP NCs films with different ligand treatments are summarized in Table 3.

Light-Emitting Devices

For light-emitting device application of NCs, ligand engineering needs to be performed more delicately, as many aspects of the NC characteristics need to be considered. The primary goal of such applications is to enhance the luminescence efficiency of NCs, which requires good passivation of the NC surface. For PL-type color-conversion application of NCs, the resulting luminescent NCs need to be well mixed with other functional elements included in color-conversion layers, such as polymer resins [70], or dispersed stably in processing solvents, which are typically polar. For electroluminescence (EL) devices (such as LEDs), charge transport is another critical factor determining the device operation. Accordingly, reducing the NC-to-NC distance is important; therefore, native ligands need to be replaced with shorter ligands or removed. However, such ligand engineering can deteriorate surface passivation and luminescence efficiency. Moreover, a reduced NC-to-NC distance (beneficial for charge transport) can enhance energy transfer between neighboring NCs in thin films, leading to the formation of a leakage pathway for excitons before the intended radiative recombination. Overall, a delicate balance between improving surface passivation, improving processability, enhancing charge transport, and preventing energy transfer needs to be attained via ligand engineering. Additionally, emphasis to any one factor alone can compromise the other factors.

Even though NCs with an InP core are the benchmark, RoHS-compliant emissive materials already employed in commercial displays, including both In and P, are oxophilic, indicating that oxidative defects such as $InPO_x$ or In_2O_3 can easily be generated even during synthesis [2, 71]. Jang et al. improved the PL quantum yield of InP-based NCs in a core/shell structure to 100% by removing these oxides via HF treatment before shell growth [72]. Subsequently, the oleic acid ligand of the as-synthesized NCs was replaced with a shorter hexanoic acid to enhance the charge transport between the NCs (Fig. 9a). Hexanoic-treated InP/ZnSe/ZnS NC LEDs exhibited a maximum brightness of 100,000 cd/m^2, an EQE of 21.4%, and an outstanding lifetime of 1,000,000 h at 100 cd/m^2 (Fig. 9b–d).

Sun et al. controlled the ligands to enhance the carrier injection from the charge-transport layer to the NC layer [73]. They replaced the DDT ligand of blue InP NCs with 1-octanethiol (OT) through a solution-state exchange method. After ligand exchange, the PLQY of the InP/ZnS/ZnS NCs in solution only decreased from 93 to 92% and the fluorescence lifetime remained constant. However, the lifetime of InP NCs in thin films decreased from 67.9 to 44.9 ns, due to the reduced NC-to-NC distance and associated enhancement in the energy transfer between NCs (Fig. 9f). Despite the degradation in luminescence characteristics, the OT-capped InP/ZnS/ZnS NC-based LEDs showed improved device performance compared to LEDs based on native NCs. With ligand engineering, the maximum luminance of the device increased from 174 cd/m^2 to 422 cd/m^2, and the current density at 6 V increased from 46 mA/cm^2 to 101 mA/cm^2 (Fig. 9g). This could be attributed to enhanced carrier injection owing to the shortened ligand. Furthermore, the maximum EQE increased from 1.8 to 2.6% (Fig. 9h), showing that ligand engineering is accompanied by a trade-off between the optoelectrical characteristics of NCs.

A key factor in enhancing LED performance is balancing the electron and hole injection from the charge transport layer [74]. For InP NC-based LEDs, the imbalance is typically due to poor hole injection, attributed to the significant energy level offset between the NC active layer and the hole transport layer. This mismatch leads to carrier recombination primarily at the edges of the emissive layers rather than its center, lowering device efficiency, increasing driving voltage, and reducing device lifetime [75, 76]. Chou et al. employed a two-step ligand exchange strategy that achieved balanced electron and hole injection into InP/ZnSe/ZnS NC films [77]. This involved replacing the native oleic acid

Table 3 Summary of the size, exchanged ligands, ligand exchange method, PCE, open-circuit voltage (V_{OC}), fill factor (FF), and short-circuit current density (J_{SC}) of PVs based on InAs and InP NCs treated with various ligands

Nanocrystal	Size (nm)	Exchanged ligands	Ligand exchange method	PCE (%)	V_{OC} (V)	FF (%)	J_{SC} (mA/cm^2)	References
InAs	5.3	MPA	Solution-state after $NOBF_4$ treatment	7.92	0.54	64.8	22.3	[39]
InAs	5.3	Br^-	Solution-state after $NOBF_4$ treatment	4.61	0.46	56.54	18.61	[39]
InP	3.2	S^{2-}	Solution-state	0.65	0.24	33	8.3	[69]
InZnP	2.8	S^{2-}	Solution-state	1.17	0.47	37	6.7	[69]

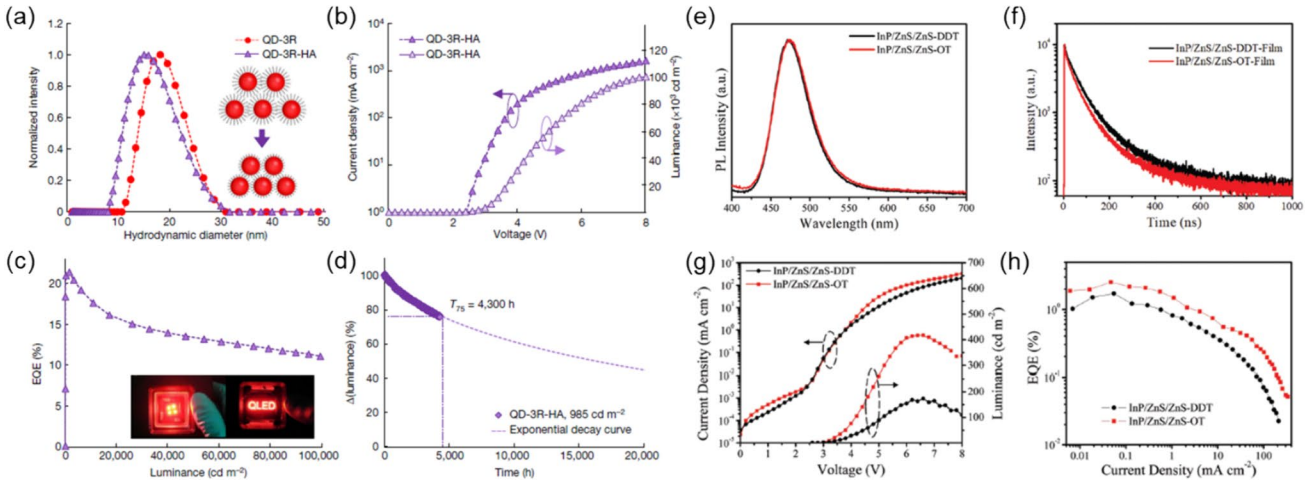

Fig. 9 **a** Dynamic laser scattering spectra of red InP/ZnSe/ZnS NCs before and after ligand exchange. **b** Current density and luminance versus voltage profiles and **c** EQE-luminance profile of NC-LEDs with ligand-exchanged NCs. **d** Lifetime measurement of the NC-LED with ligand-exchanged NCs fitted with exponential decay curve. Reprinted with permission from Ref. [72]. Copyright 2019, Springer Nature Limited. **e** Photoluminescence and **f** time-resolved PL decay traces of InP/ZnSe/ZnS NCs with different ligands. **g** Current density–voltage-luminance (*J-V-L*) characteristics and **h** EQE-*J* characteristics of NC-LEDs before and after ligand exchange. Reprinted with permission from Ref. [73]. Copyright 2022, Wiley–VCH GmbH

ligands with 1,4-butanediamine (BDA), adjusting the conduction band from 3.55 eV to 3.58 eV and the valence band from 5.80 eV to 5.79 eV. Electrical analysis through hole-only (HOD) and electron-only devices (EOD) confirmed that this substitution suppressed electron injection and enhanced hole injection. Further treatment with ZnI_2 improved hole injection and transport by passivating residual hole traps on the NC surface. The resulting LEDs, treated with BDA and ZnI_2, exhibited a maximum brightness of 12,646 cd/m^2 and an EQE of 16.3%.

Kwak et al. demonstrated that semiconducting diblock copolymer ligands could balance electron and hole injection while also reducing Förster resonance energy transfer (FRET) between emissive NCs [78]. Specifically, the researchers partially exchanged the native oleic acid ligands of NCs with (poly(9-4-vinylbenzyl)-carbazole-block-cysteaminemethyldisulfide), containing carbazole and disulfide anchoring groups. The use of carbazole groups in the copolymeric ligand facilitated hole injection and suppressed electron injection to NCs [79], leading to a more balanced charge injection. Moreover, the increased steric hindrance provided by the bulky copolymer ligands separated NCs from each other and suppressed FRET that typically hinders radiative recombination and reduces device efficiency. Consequently, copolymer-treated InP/ZnSeS/ZnS NC LEDs exhibited superior performance ($EQE_{max} = 3.7\%$ and maximum brightness = 4500 cd/m^2) compared to pristine devices ($EQE_{max} = 2.5\%$ and maximum brightness = 4200 cd/m^2).

Furthermore, the same research group developed a strategy to improve the operational stability of NC LEDs through ligand engineering [80]. They explored the effect of excess carriers on the degradation of InP/ZnSe/ZnS NC LEDs by introducing a thin poly(methyl methacrylate) (PMMA) layer between one of the charge transport layers and the emissive NC layer, creating unbalanced charge devices. Notably, significant degradation in the electroluminescence characteristics was observed only in devices with excessive holes, attributed to the generation of oxidative surface defects on NCs and the dissociation of native oleate ligands [81]. To mitigate degradation, hexylamine ligands were introduced, which bind robustly to the NC surface and are electrochemically stable against oxidation [82]. InP/ZnSe/ZnS NC LEDs treated with hexylamine demonstrated a higher maximum luminescence of 36,540 cd/m^2 and a longer half-life of 72,757 h, compared to pristine NC LEDs which showed 14,650 cd/m^2 and 667 h. Detailed comparisons of device characteristics across different InP-based NCs with various ligand treatments are summarized in Table 4.

High-resolution patterning of NCs is another important aspect for realizing NC-based displays. Among the many different patterning methods reported, including transfer printing [83–87] and inkjet printing [88–92], photolithography, which is widely employed in the semiconductor/display industry [93–95], is a promising method that can produce micrometre-scale NC patterns that meet the rigorous standards in the industry in terms of reproducibility and throughput rate. To employ photolithography, NCs must be photoactive, and imparting photoactivity to NCs typically requires ligand engineering.

Talapin et al. reported a direct photopatterning method for NC films using UV active ion-pair ligand systems (Cat^+X^-)

Table 4 Summary of the PL peak, PL QY, exchanged ligands, ligand exchange method, EQE_{max}, L_{max}, and lifetime of LEDs based on InP NCs treated with various ligands

Nanocrystal	PL peak (nm)	PL QY (%)	Exchanged ligands	Ligand exchange method	EQE_{max} (%)	L_{max} (cd/m^2)	Lifetime	References
InP/ZnSe/ZnS	630	100	Oleic acid (Native)	–	18.0	70,718	T_{75} = 3000 h at 1000 cd/m^2	[72]
InP/ZnSe/ZnS	630	100	Hexanoic acid	Solution-state	21.4	100,000	T_{50} = 1,000,000 h at 100 cd/m^2	[72]
InP/ZnS/ZnS	488	93	DDT (Native)	–	1.8	174	N/A	[73]
InP/ZnS/ZnS	488	92	OT	Solution-state	2.6	422	N/A	[73]
InP/ZnSe/ZnS	535	86	Oleic acid (Native)	–	5.7	3427	T_{50} = 373.9 h at 100 cd/m^2	[77]
InP/ZnSe/ZnS	540	86	BDA	Solution-state	8.5	14,287	T_{50} = 545.8 h at 100 cd/m^2	[77]
InP/ZnSe/ZnS	540	86	BDA + I^-	Solution-state	16.3	12,646	T_{50} = 1033.4 h at 100 cd/m^2	[77]
InP/ZnSeS/ZnS	631	N/A	Oleic acid (Native)	–	2.5	4200	T_{50} = 30 h at 1000 cd/m^2	[78]
InP/ZnSeS/ZnS	631	N/A	Semiconducting diblock copolymer*	Solution-state	3.7	4500	T_{50} = 7600 h at 100 cd/m^2	[78]
InP/ZnSe/ZnS	N/A	N/A	Oleic acid (Native)	–	N/A	14,650	T_{50} = 667 h at 100 cd/m^2	[80]
InP/ZnSe/ZnS	N/A	N/A	Hexylamine	Solution-state	N/A	36,540	T_{50} = 72,757 h at 100 cd/m^2	[80]

*Poly(9-(4-vinylbenzyl)-carbazole-block-cysteaminemethyldisulfide

[96]. These ligands consist of a photosensitive cation (possessing photo acid generator (PAG) moieties) and surface-binding inorganic anion. Alternatively, a ligand system containing photosensitive anions that could directly decompose and change the solubility of the NC film was introduced. By harnessing UV-induced solubility changes, NC patterns can be formed by selectively dissolving the unwanted regime of NC films. The generated NC patterns showed a low dissolution rate compared to the original solvent used to cast the film. Hence, the structure of the pattern was maintained during the repeated NC patterning processes. Accordingly, red (R), green (G), and blue (B) multilayer patterns were successfully formed. Researchers have demonstrated that this strategy can be applied not only to InP/ZnS NCs but also to blue-emitting ZnSe/ZnS NCs, as well as metal or metal oxide nanoparticles, as long as functional ligands can be attached.

However, even with a small amount of PAG, the PLQY of the NCs decreased significantly [97]. Cho et al. demonstrated a strategy to recover the decrease in PLQY that occurs during the patterning process [98]. They used 2-(4-methoxystyryl)-4,6-bis(trichloromethyl)-1,3,5-triazine (MBT), which allows for a relatively lower UV dose and enables a smaller PLQY reduction than other types of PAGs. When the NC/MBT films were irradiated with UV light, in situ ligand exchange occurred, leading to a small amount of carboxylate ligands being replaced with chloride ligands on the NC surface (Fig. 10a). Because these chloride ligands form deep trap states and cause a decrease in the PLQY (~ 18% compared to the pristine NC film) [99], the chloride ligands were re-exchanged with amine/carboxylate pair ligands through a solid-state exchange method, referred to as the ligand pair treatment (LPT) method (Fig. 10b). The recovery of the PLQY was confirmed via exchange with longer amine/carboxylate pair ligands (Fig. 10c). As a result, NC patterns at a scale of 1 μm were obtained, with the PLQY recovering 70% of its original value obtained from pristine NC films (Fig. 10e).

Bang et al. demonstrated that polymeric ligands with UV-induced crosslinking can be utilized for the direct photopatterning of NCs [100]. They introduced (poly(vinyltriphenylamine-random-azidostytene) (PTPA-N_3-SH), which contains two units: one with azide groups that can undergo UV-induced crosslinking reactions needed for photopatterning and the other with triphenylamine to allow hole transport [101, 102]. They demonstrated that PTPA-N_3-SH-capped NCs can be used to generate RGB (green-InP NCs) full-color micropatterns scaled down to ~ 10 μm. PTPA-N_3-SH is also applicable for metallic nanoparticles (NPs). The same group expanded their strategy to introduce polymer ligands containing cinnamoyl groups that could be activated under a 365 nm UV light source into perovskite

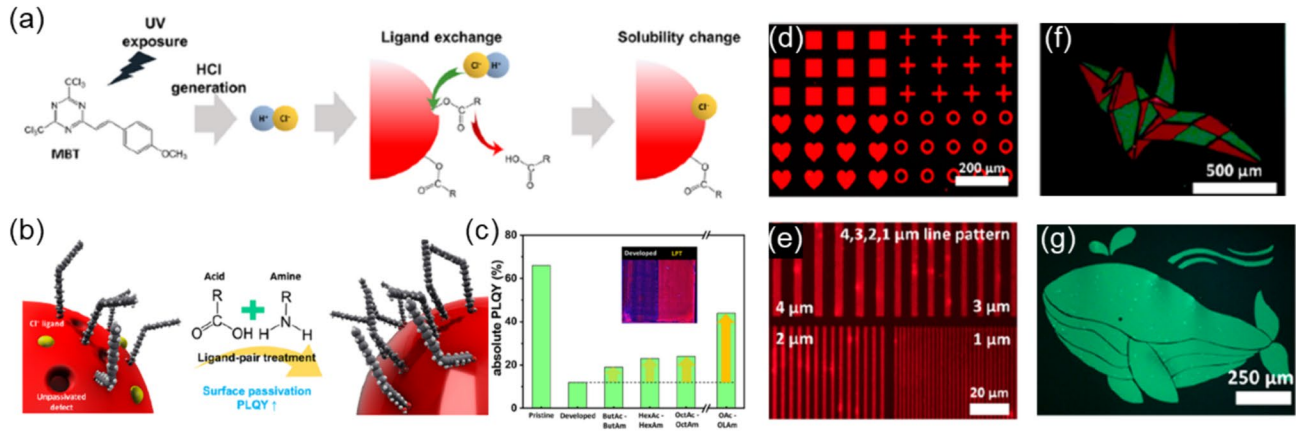

Fig. 10 Schematic description of **a** in situ ligand exchange and **b** LPT strategy for surface re-passivation. **c** PLQY change of InP NC films caused by LPT with ligands of varying chain lengths. Fluorescence optical image of **d** various shapes, **e** line patterns (1 ~ 4 μm), **f** red-green dual-color crane, and **g** green whale patterns based on InP NCs. Reprinted with permission from Ref. [98]. Copyright 2023 American Chemical Society

NC patterning [103]. In addition, they also demonstrated polymeric ligands containing poly(glycidyl methacrylate) groups that could be activated with a Lewis acid catalyst to enhance the chemical resistance and thermal stability of NCs [104].

Lee et al. identifies a ligand that facilitates the use of environmentally friendly solvents for patterning InP/$ZnSe_xS_{1-x}$ NCs. Specifically, mono-2-(methacryloyloxyl) ethyl succinate (MMES) ligand, which has an acrylate and carboxylic acid end group, is insoluble in carcinogenic or neurotoxic organic solvents, such as toluene and hexane, but soluble in environmentally benign polar solvents, such as ethanol, isopropanol, and propylene glycol methyl ether acetate (PGMEA) [31]. Researchers have utilized MMES-capped NCs for inkjet patterning owing to the excellent colloidal and thermal stabilities of NC inks. Furthermore, the resulting MMES-capped NCs were mixed well with photocrosslinkable resins (bisphenol A ethoxylated diacrylate with the photoinitiator Irgacure Oxo-02). Using this mixture, the researchers demonstrated the direct photopatterning of InP/$ZnSe_xS_{1-x}$ NCs.

Bae et al. demonstrated a direct photopatterning method by introducing photo-crosslinkable ligands (PXLs) (Fig. 11a) [105]. PXLs containing benzophenone derivatives underwent photo-crosslinking reactions with neighboring aliphatic chains under a 365 nm UV illumination (Fig. 11c). Because the NC films could be crosslinked completely using less than 10 mol% of PXLs (among all ligands), dual-ligand passivation of NCs was possible. This permitted controlling the solubility of the NCs in various solvents by controlling the remaining ligands (dispersing ligands (DLs)) (> 90 mol%) (Fig. 11b). Consequently, NCs were successfully dispersed in both polar and nonpolar solvents, such as PGMEA, diethylene glycol monoethyl ether acetate (DGMEA), and trifluorotoluene (Fig. 11d). The photo-crosslinked NC films exhibited chemical durability while preserving the intrinsic PL and electroluminescence (EL) properties of the pristine NC films. Ultra-high resolution (exceeding 15,000 p.p.i.) RGB NC patterns were successfully fabricated (Fig. 11e), and the fabrication of a 10 × 10 passive matrix-driven RGB NC-LED array based on this photopatterning was demonstrated (Fig. 11f).

Conclusion and Perspectives

We aimed to provide a comprehensive review of the relationship between ligand engineering and the physical properties of this emerging class of materials systems that are the InP and InAs NCs. As explained above, ligands on the surface of NCs significantly impact their physical properties, ranging from structural characteristics such as shape or size, to material processability aspects including colloidal stability, solubility in different solvents, surface energy, and photopatternability. Furthermore, ligands influence the positioning of energy levels, luminescent characteristics, and electrical transport properties of NCs. Therefore, precise control over ligands is pivotal in enhancing the performance of electronic and optoelectronic devices based on NC thin films. However, it is essential to underscore that efforts to improve one aspect of these materials often lead to degradation in others, resulting in trade-offs in the resultant characteristics post-ligand engineering. For instance, strategies aimed at enhancing transport characteristics often involve replacing long ligands with shorter ones to improve coupling between NCs. While this enhances electrical transport, it typically leads to poorer luminescence due to inadequate passivation of dangling bonds by the shorter ligands. Similarly, improving the

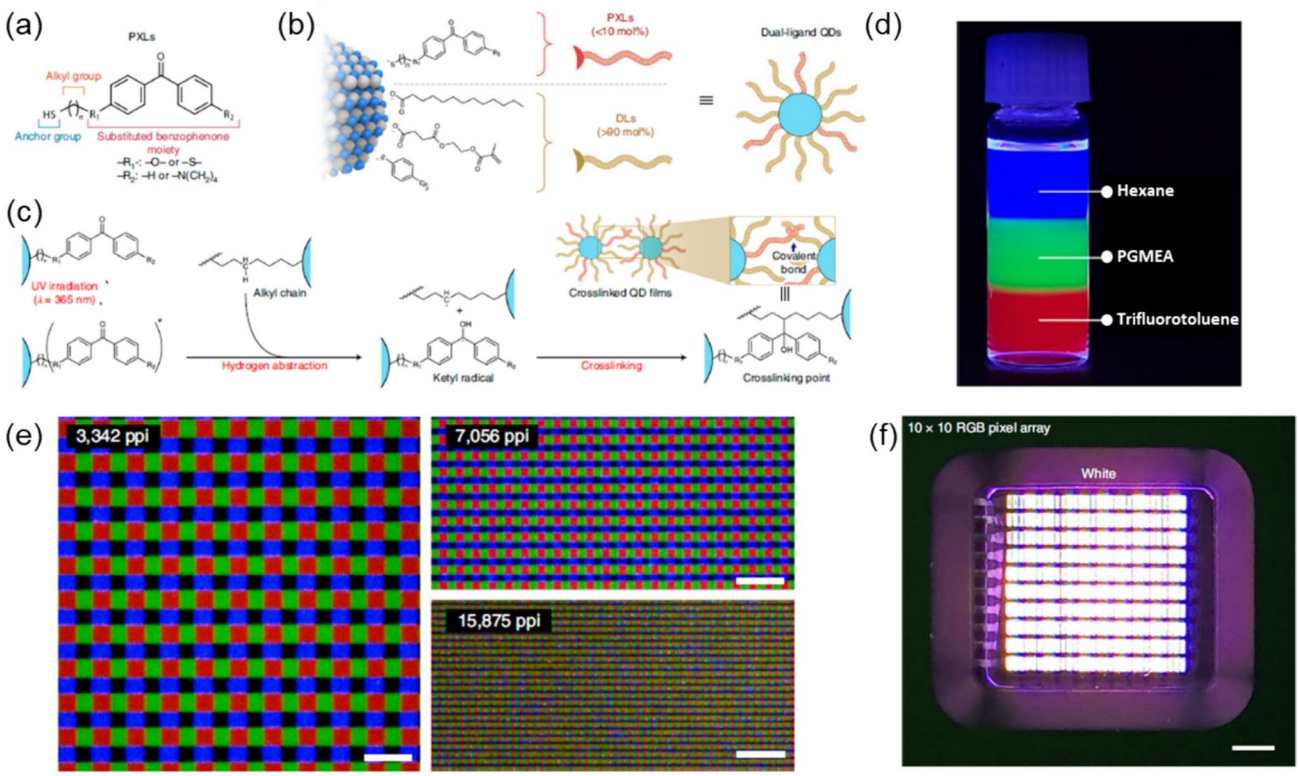

Fig. 11 **a** Chemical structure of PXLs. **b** Schematic of dual-ligand NCs. **c** Schematic description of photocrosslinking between dual-ligand NCs. **d** Photograph of dual-ligand RGB NC dispersions in trifluorotoluene, PGMEA, and hexane. **e** Fluorescence optical images of ultra-high resolution RGB NC patterns. **f** Electroluminescent images of 10×10 RGB NC-LED arrays. Reprinted with permission from Ref. [105]. Copyright 2022, Springer Nature Limited

colloidal stability of NCs, usually achieved through ligands that provide good steric hindrance, can result in diminished transport characteristics. While separate ligand engineering approaches are necessary to develop the specific material characteristics of In-based III–V semiconductor NCs, these strategies must also consider the varied impacts of ligand engineering on the NCs as a whole. The practical application of these semiconductor NCs relies on such understanding.

Acknowledgements This work was supported by the National Research Foundation of Korea (NRF) grant funded by the Ministry of Science, ICT, and Future Planning (2021R1A2C2008332 and 2021M3H4A3A01062964).

References

1. F.P. García de Arquer, D.V. Talapin, V.I. Klimov, Y. Arakawa, M. Bayer, E.H. Sargent, Science **373**, eaaz8541 (2021)
2. P. Reiss, M. Carrière, C. Lincheneau, L. Vaure, S. Tamang, Chem. Rev. **116**, 10731–10819 (2016)
3. M. Liu, N. Yazdani, M. Yarema, M. Jansen, V. Wood, E.H. Sargent, Nat. Electron. **4**, 548–558 (2021)
4. X. Dai, Y. Deng, X. Peng, Y. Jin, Adv. Mater. **29**, 1607022 (2017)
5. H.B. Jalali, L.D. Trizio, L. Manna, F.D. Stasio, Chem. Soc. Rev. **51**, 9861–9881 (2022)
6. T. Kim, D. Shin, M. Kim, H. Kim, E. Cho, M. Choi, J. Kim, E. Jang, S. Jeong, ACS Energy Lett. **8**, 447–456 (2023)
7. Y. Kim, J.H. Chang, H. Choi, Y.-H. Kim, W.K. Bae, S. Jeong, Chem. Sci. **11**, 913–922 (2020)
8. E. Cho, T. Kim, S.-M. Choi, H. Jang, K. Min, E. Jang, ACS Appl. Nano Mater. **1**, 7106–7114 (2018)
9. M.A. Boles, D. Ling, T. Hyeon, D.V. Talapin, Nat. Mater. **15**, 141–153 (2016)
10. R.G. Pearson, J. Am. Chem. Soc. **85**, 3533–3539 (1963)
11. S. Tamang, C. Lincheneau, Y. Hermans, S. Jeong, P. Reiss, Chem. Mater. **28**, 2491–2506 (2016)
12. D. Battaglia, X. Peng, Nano Lett. **2**, 1027–1030 (2002)
13. J. Ouyang, J. Kuijper, S. Brot, D. Kingston, X. Wu, D.M. Leek, M.Z. Hu, J.A. Ripmeester, K. Yu, J. Phys. Chem. C **113**, 7579–7593 (2009)
14. K. De Nolf, R.K. Capek, S. Abe, M. Sluydts, Y. Jang, J.C. Martins, S. Cottenier, E. Lifshitz, Z. Hens, J. Am. Chem. Soc. **137**, 2495–2505 (2015)
15. C.W. Hoerr, R.S. Sedgwick, A.W. Ralston, J. Org. Chem. **11**, 603–609 (1946)
16. Z. Zhuang, X. Lu, Q. Peng, Y. Li, Chem. Eur. J. **17**, 10445–10452 (2011)
17. M. Biondi, M.-J. Choi, Z. Wang, M. Wei, S. Lee, H. Choubisa, L.K. Sagar, B. Sun, S.-W. Baek, B. Chen, P. Todorović, A.M. Najarian, A.S. Rasouli, D.-H. Nam, M. Vafaie, Y.C. Li, K.

Bertens, S. Hoogland, O. Voznyy, F.P. García de Arquer, E.H. Sargent, Adv. Mater. **33**, 2101056 (2021)
18. S.-H. Kim, D. Lee, S. Moon, J.-H. Choi, D. Kim, J. Kim, S.-W. Baek, Adv. Funct. Mater. **33**, 2303778 (2023)
19. Z. Liu, R. Pascazio, L. Goldoni, D. Maggioni, D. Zhu, Y.P. Ivanov, G. Divitini, J.L. Camarelles, H.B. Jalali, I. Infante, L. De Trizio, L. Manna, J. Am. Chem. Soc. **145**, 18329–18339 (2023)
20. D. Zhu, F. Bellato, H.B. Jalali, F.D. Stasio, M. Prato, Y.P. Ivanov, G. Divitini, I. Infante, L. De Trizio, L. Manna, J. Am. Chem. Soc. **144**, 10515–10523 (2022)
21. J. Lim, W.K. Bae, K.U. Park, L.Z. Borg, R. Zentel, S. Lee, K. Char, Chem. Mater. **25**, 1443–1449 (2013)
22. D. Kim, Y.K. Lee, D. Lee, W.D. Kim, W.K. Bae, D.C. Lee, ACS Nano **11**, 12461–12472 (2017)
23. D.-E. Yoon, W.D. Kim, D. Kim, D. Lee, S. Koh, W.K. Bae, D.C. Lee, J. Phys. Chem. C **121**, 24837–24844 (2017)
24. S. Koh, W.D. Kim, W.K. Bae, Y.K. Lee, D.C. Lee, Chem. Mater. **31**, 1990–2001 (2019)
25. A. Narayanaswamy, H. Xu, N. Pradhan, M. Kim, X. Peng, J. Am. Chem. Soc. **128**, 10310–10319 (2006)
26. W.W. Yu, Y.A. Wang, X. Peng, Chem. Mater. **15**, 4300–4308 (2003)
27. P.M. Allen, B.J. Walker, M.G. Bawendi, Angew. Chem. Int. Ed. **49**, 760–762 (2010)
28. Y. Yang, H. Qin, M. Jiang, L. Lin, T. Fu, X. Dai, Z. Zhang, Y. Niu, H. Cao, Y. Jin, F. Zhao, X. Peng, Nano Lett. **16**, 2133–2138 (2016)
29. D. Kim, W.D. Kim, M.S. Kang, S.-H. Kim, D.C. Lee, Nano Lett. **15**, 714–720 (2015)
30. D. Kim, W.K. Bae, S.-H. Kim, D.C. Lee, Nano Lett. **19**, 963–970 (2019)
31. D. Hahm, J. Park, I. Jeong, S. Rhee, T. Lee, C. Lee, S. Chung, W.K. Bae, S. Lee, ACS Appl. Mater. Interfaces. **12**, 10563–10570 (2020)
32. D.J. Chadi, Phys. Rev. Lett. **43**, 43–47 (1979)
33. T. Kang, K. Um, J. Park, H. Chang, D.C. Lee, C.-K. Kim, K. Lee, Sens. Actuators B Chem. **222**, 871–878 (2016)
34. N. Wang, S. Koh, B.G. Jeong, D. Lee, W.D. Kim, K. Park, M.K. Nam, K. Lee, Y. Kim, B.-H. Lee, K. Lee, W.K. Bae, D.C. Lee, Nanotechnology **28**, 185603 (2017)
35. J.-H. Ko, D. Yoo, Y.-H. Kim, Chem. Commun. **53**, 388–391 (2017)
36. H. Goodman, L. Mei, T.L. Gianetti, Front. Chem. **7**, 365 (2019). https://doi.org/10.3389/fchem.2019.00365
37. J. Owen, Science **347**, 615–616 (2015)
38. P.R. Brown, D. Kim, R.R. Lunt, N. Zhao, M.G. Bawendi, J.C. Grossman, V. Bulović, ACS Nano **8**, 5863–5872 (2014)
39. J.H. Song, H. Choi, H.T. Pham, S. Jeong, Nat. Commun. **9**, 4267 (2018)
40. C.R. Kagan, C.B. Murray, Nat. Nanotechnol. **10**, 1013–1026 (2015)
41. A. Nag, M.V. Kovalenko, J.-S. Lee, W. Liu, B. Spokoyny, D.V. Talapin, J. Am. Chem. Soc. **133**, 10612–10620 (2011)
42. S.M. Geyer, P.M. Allen, L.-Y. Chang, C.R. Wong, T.P. Osedach, N. Zhao, V. Bulovic, M.G. Bawendi, ACS Nano **4**, 7373–7378 (2010)
43. D.C. Tripathi, L. Asor, G. Zaharoni, U. Banin, N. Tessler, J. Phys. Chem. C **123**, 18717–18725 (2019)
44. L. Asor, J. Liu, Y. Ossia, D.C. Tripathi, N. Tessler, A.I. Frenkel, U. Banin, Adv. Funct. Mater. **31**, 2007456 (2021)
45. L. Asor, J. Liu, S. Xiang, N. Tessler, A.I. Frenkel, U. Banin, Adv. Mater. **35**, 2208332 (2023)
46. J.I. Yoon, H. Kim, M. Kim, H. Cho, Y.A. Kwon, M. Choi, S. Park, T. Kim, S. Lee, H. Jo, B. Kim, J.H. Cho, J.-S. Park, S. Jeong, M.S. Kang, Sci. Adv. **9**, eadj8276 (2023)
47. T.-G. Kim, D. Zherebetskyy, Y. Bekenstein, M.H. Oh, L.-W. Wang, E. Jang, A.P. Alivisatos, ACS Nano **12**, 11529–11540 (2018)
48. W. Liu, J.-S. Lee, D.V. Talapin, J. Am. Chem. Soc. **135**, 1349–1357 (2013)
49. J. Jang, W. Liu, J.S. Son, D.V. Talapin, Nano Lett. **14**, 653–662 (2014)
50. H. Zhang, J. Jang, W. Liu, D.V. Talapin, ACS Nano **8**, 7359–7369 (2014)
51. M. Scheele, J.H. Engel, V.E. Ferry, D. Hanifi, Y. Liu, A.P. Alivisatos, ACS Nano **7**, 6774–6781 (2013)
52. T. Zhao, N. Oh, D. Jishkariani, M. Zhang, H. Wang, N. Li, J.D. Lee, C. Zeng, M. Muduli, H.-J. Choi, D. Su, C.B. Murray, C.R. Kagan, J. Am. Chem. Soc. **141**, 15145–15152 (2019)
53. T. Zhao, Q. Zhao, J. Lee, S. Yang, H. Wang, M.-Y. Chuang, Y. He, S.M. Thompson, G. Liu, N. Oh, C.B. Murray, C.R. Kagan, Chem. Mater. **34**, 8306–8315 (2022)
54. A. Dong, X. Ye, J. Chen, Y. Kang, T. Gordon, J.M. Kikkawa, C.B. Murray, J. Am. Chem. Soc. **133**, 998–1006 (2011)
55. M.-J. Si, S. Jee, M. Yang, D. Kim, Y. Ahn, S. Lee, C. Kim, I.-H. Bae, S.-W. Baek, Adv. Sci. **11**, 2306798 (2024)
56. S. Lee, M.-J. Choi, G. Sharma, M. Biondi, B. Chen, S.-W. Baek, A.M. Najarian, M. Vafaie, J. Wicks, L.K. Sagar, S. Hoogland, F.P.G. de Arquer, O. Voznyy, E.H. Sargent, Nat. Commun. **11**, 4814 (2020)
57. H.-S. Jeong, D. Kim, S. Jee, M.-J. Si, C. Kim, J.-Y. Lee, Y. Jung, S.-W. Baek, Int. J. Energy Res. **2023**, 4911750 (2023)
58. M. Liu, F. Che, B. Sun, O. Voznyy, A. Proppe, R. Munir, M. Wei, R. Quintero-Bermudez, L. Hu, S. Hoogland, A. Mandelis, A. Amassian, S.O. Kelley, F.P. García de Arquer, E.H. Sargent, ACS Energy Lett. **4**, 1225–1230 (2019)
59. D. Zherebetskyy, Y. Zhang, M. Salmeron, L.-W. Wang, J. Phys. Chem. Lett. **6**, 4711–4716 (2015)
60. Y. Li, X. Hou, X. Dai, Z. Yao, L. Lv, Y. Jin, X. Peng, J. Am. Chem. Soc. **141**, 6448–6452 (2019)
61. M.-J. Choi, L.K. Sagar, B. Sun, M. Biondi, S. Lee, A.M. Najjariyan, L. Levina, F.P. García de Arquer, E.H. Sargent, Nano Lett. **21**, 6057–6063 (2021)
62. B. Sun, A.M. Najarian, L.K. Sagar, M. Biondi, M.-J. Choi, X. Li, L. Levina, S.-W. Baek, C. Zheng, S. Lee, A.R. Kirmani, R. Sabatini, J. Abed, M. Liu, M. Vafaie, P. Li, L.J. Richter, O. Voznyy, M. Chekini, Z.-H. Lu, F.P. García de Arquer, E.H. Sargent, Adv. Mater. **34**, 2203039 (2022)
63. P. Xia, B. Sun, M. Biondi, J. Xu, O. Atan, M. Imran, Y. Hassan, Y. Liu, J.M. Pina, A.M. Najarian, L. Grater, K. Bertens, L.K. Sagar, H. Anwar, M.-J. Choi, Y. Zhang, M. Hasham, F.P. García de Arquer, S. Hoogland, M.W.B. Wilson, E.H. Sargent, Adv. Mater. **35**, 2301842 (2023)
64. B.K. Jung, H. Yoo, B. Seo, H.J. Choi, Y.K. Choi, T.H. Kim, N. Oh, S.Y. Kim, S. Kim, Y. Lee, J.W. Shim, H.Y. Park, G.W. Hwang, T.N. Ng, S.J. Oh, ACS Energy Lett. **9**, 504–512 (2024)
65. J. Leemans, V. Pejović, E. Georgitzikis, M. Minjauw, A.B. Siddik, Y.-H. Deng, Y. Kuang, G. Roelkens, C. Detavernier, I. Lieberman, P.E. Malinowski, D. Cheyns, Z. Hens, Adv. Sci. **9**, 2200844 (2022)
66. J. Leemans, K.C. Dümbgen, M.M. Minjauw, Q. Zhao, A. Vantomme, I. Infante, C. Detavernier, Z. Hens, J. Am. Chem. Soc. **143**, 4290–4301 (2021)
67. K.C. Dümbgen, J. Leemans, V. De Roo, M. Minjauw, C. Detavernier, Z. Hens, Chem. Mater. **35**, 1037–1046 (2023)
68. J.-H. Kim, B.K. Jung, S.-K. Kim, K.-R. Yun, J. Ahn, S. Oh, M.-G. Jeon, T.-J. Lee, S. Kim, N. Oh, S.J. Oh, T.-Y. Seong, Adv. Sci. **10**, 2207526 (2023)
69. R.W. Crisp, N. Kirkwood, G. Grimaldi, S. Kinge, L.D.A. Siebbeles, A.J. Houtepen, ACS Appl. Energy Mater. **1**, 6569–6576 (2018)

70. Y.H. Kim, S. Koh, H. Lee, S.-M. Kang, D.C. Lee, B.-S. Bae, ACS Appl. Mater. Interfaces. **12**, 3961–3968 (2020)
71. J.L. Stein, W.M. Holden, A. Venkatesh, M.E. Mundy, A.J. Rossini, G.T. Seidler, B.M. Cossairt, Chem. Mater. **30**, 6377–6388 (2018)
72. Y.-H. Won, O. Cho, T. Kim, D.-Y. Chung, T. Kim, H. Chung, H. Jang, J. Lee, D. Kim, E. Jang, Nature **575**, 634–638 (2019)
73. W. Zhang, Y. Tan, X. Duan, F. Zhao, H. Liu, W. Chen, P. Liu, X. Liu, K. Wang, Z. Zhang, X.W. Sun, Adv. Opt. Mater. **10**, 2200685 (2022)
74. Y. Lee, B.G. Jeong, H. Roh, J. Roh, J. Han, D.C. Lee, W.K. Bae, J.-Y. Kim, C. Lee, Adv. Quantum Technol. **1**, 1700006 (2018)
75. S. Chen, X. Jiang, F. So, Org. Electron. **14**, 2518–2522 (2013)
76. C. Coburn, S.R. Forrest, Phys. Rev. Appl. **7**, 041002 (2017)
77. W.-C. Chao, T.-H. Chiang, Y.-C. Liu, Z.-X. Huang, C.-C. Liao, C.-H. Chu, C.-H. Wang, H.-W. Tseng, W.-Y. Hung, P.-T. Chou, Commun. Mater. **2**, 96 (2021)
78. Y. Park, B. Klöckner, D. Hahm, J. Kim, T. Lee, J. Kim, W.K. Bae, R. Zentel, J. Kwak, J. Mater. Chem. C **9**, 10398–10405 (2021)
79. A. Fokina, Y. Lee, J.H. Chang, M. Park, Y. Sung, W.K. Bae, K. Char, C. Lee, R. Zentel, Adv. Mater. Interfaces **3**, 1600279 (2016)
80. K. Kim, D. Hahm, G.W. Baek, T. Lee, D. Shin, J. Lim, W.K. Bae, J. Kwak, ACS Appl. Electron. Mater. **4**, 6229–6236 (2022)
81. K.E. Shulenberger, H.R. Keller, L.M. Pellows, N.L. Brown, G. Dukovic, J. Phys. Chem. C **125**, 22650–22659 (2021)
82. C. Pu, X. Dai, Y. Shu, M. Zhu, Y. Deng, Y. Jin, X. Peng, Nat. Commun. **11**, 937 (2020)
83. T.W. Nam, M. Kim, Y. Wang, G.Y. Kim, W. Choi, H. Lim, K.M. Song, M.-J. Choi, D.Y. Jeon, J.C. Grossman, Y.S. Jung, Nat. Commun. **11**, 3040 (2020)
84. M.K. Choi, J. Yang, D.C. Kim, Z. Dai, J. Kim, H. Seung, V.S. Kale, S.J. Sung, C.R. Park, N. Lu, T. Hyeon, D.-H. Kim, Adv. Mater. **30**, 1703279 (2018)
85. B.H. Kim, S. Nam, N. Oh, S.-Y. Cho, K.J. Yu, C.H. Lee, J. Zhang, K. Deshpande, P. Trefonas, J.-H. Kim, J. Lee, J.H. Shin, Y. Yu, J.B. Lim, S.M. Won, Y.K. Cho, N.H. Kim, K.J. Seo, H. Lee, T.-I. Kim, M. Shim, J.A. Rogers, ACS Nano **10**, 4920–4925 (2016)
86. H. Cho, J. Kwak, J. Lim, M. Park, D. Lee, W.K. Bae, Y.S. Kim, K. Char, S. Lee, C. Lee, ACS Appl. Mater. Interfaces. **7**, 10828–10833 (2015)
87. T.-H. Kim, D.-Y. Chung, J. Ku, I. Song, S. Sul, D.-H. Kim, K.-S. Cho, B.L. Choi, J.M. Kim, S. Hwang, K. Kim, Nat. Commun. **4**, 2637 (2013)
88. G. Zhang, H. Zhang, R. Yu, Y. Duan, Y. Huang, Z. Yin, A.C.S. Appl, Mater. Interfaces. **14**, 14712–14720 (2022)
89. P. Yang, L. Zhang, D.J. Kang, R. Strahl, T. Kraus, Adv. Opt. Mater. **8**, 1901429 (2020)
90. C. Wei, W. Su, J. Li, B. Xu, Q. Shan, Y. Wu, F. Zhang, M. Luo, H. Xiang, Z. Cui, H. Zeng, Adv. Mater. **34**, 2107798 (2022)
91. H. Roh, D. Ko, D.Y. Shin, J.H. Chang, D. Hahm, W.K. Bae, C. Lee, J.Y. Kim, J. Kwak, Adv. Opt. Mater. **9**, 2002129 (2021)
92. Y. Liu, F. Li, Z. Xu, C. Zheng, T. Guo, X. Xie, L. Qian, D. Fu, X. Yan, ACS Appl. Mater. Interfaces. **9**, 25506–25512 (2017)
93. W.-B. Jung, S. Jang, S.-Y. Cho, H.-J. Jeon, H.-T. Jung, Adv. Mater. **32**, 1907101 (2020)
94. D.P. Sanders, Chem. Rev. **110**, 321–360 (2010)
95. T. Ito, S. Okazaki, Nature **406**, 1027–1031 (2000)
96. Y. Wang, I. Fedin, H. Zhang, D.V. Talapin, Science **357**, 385–388 (2017)
97. H. Cho, J.-A. Pan, H. Wu, X. Lan, I. Coropceanu, Y. Wang, W. Cho, E.A. Hill, J.S. Anderson, D.V. Talapin, Adv. Mater. **32**, 2003805 (2020)
98. J. Lee, J. Ha, H. Lee, H. Cho, D.C. Lee, D.V. Talapin, H. Cho, ACS Energy Lett. **8**, 4210–4217 (2023)
99. V. Sayevich, C. Guhrenz, M. Sin, V.M. Dzhagan, A. Weiz, D. Kasemann, E. Brunner, M. Ruck, D.R.T. Zahn, K. Leo, N. Gaponik, A. Eychmüller, Adv. Funct. Mater. **26**, 2163–2175 (2016)
100. J. Ko, J.H. Chang, B.G. Jeong, H.J. Kim, J.F. Joung, S. Park, D.H. Choi, W.K. Bae, J. Bang, ACS Appl. Mater. Interfaces. **12**, 42153–42160 (2020)
101. J. Kwak, W.K. Bae, M. Zorn, H. Woo, H. Yoon, J. Lim, S.W. Kang, S. Weber, H.-J. Butt, R. Zentel, S. Lee, K. Char, C. Lee, Adv. Mater. **21**, 5022–5026 (2009)
102. M. Zorn, W.K. Bae, J. Kwak, H. Lee, C. Lee, R. Zentel, K. Char, ACS Nano **3**, 1063–1068 (2009)
103. J. Ko, K. Ma, J.F. Joung, S. Park, J. Bang, Nano Lett. **21**, 2288–2295 (2021)
104. J. Ko, B.G. Jeong, J.H. Chang, J.F. Joung, S.-Y. Yoon, D.C. Lee, S. Park, J. Huh, H. Yang, W.K. Bae, S.G. Jang, J. Bang, NPG Asia Mater. **12**, 19 (2020)
105. D. Hahm, J. Lim, H. Kim, J.-W. Shin, S. Hwang, S. Rhee, J.H. Chang, J. Yang, C.H. Lim, H. Jo, B. Choi, N.S. Cho, Y.-S. Park, D.C. Lee, E. Hwang, S. Chung, C.-M. Kang, M.S. Kang, W.K. Bae, Nat. Nanotechnol. **17**, 952–958 (2022)